

## Topical Review: Development of overgrown semi-polar GaN for high efficiency green/yellow emission

This content has been downloaded from IOPscience. Please scroll down to see the full text.

2016 Semicond. Sci. Technol. 31 093003

(<http://iopscience.iop.org/0268-1242/31/9/093003>)

View [the table of contents for this issue](#), or go to the [journal homepage](#) for more

### Download details:

IP Address: 143.167.181.146

This content was downloaded on 12/09/2016 at 10:54

Please note that [terms and conditions apply](#).

You may also be interested in:

[Recent progress in metal-organic chemical vapor deposition of \(0001\) N-polar group-III nitrides](#)

Stacia Keller, Haoran Li, Matthew Laurent et al.

[GaN-based light-emitting diodes on various substrates: a critical review](#)

Guoqiang Li, Wenliang Wang, Weijia Yang et al.

[Prospects of III-nitride optoelectronics grown on Si](#)

D Zhu, D J Wallis and C J Humphreys

[Metal organic vapour phase epitaxy](#)

Pierre Gibart

[Semipolar GaN grown on foreign substrates](#)

F Scholz

[Yellow–red emission from \(Ga,In\)N heterostructures](#)

B Damilano and B Gil

[Nitride-based laser diodes grown by plasma-assisted molecular beam epitaxy](#)

C Skierbiszewski, H Turski, G Muziol et al.

## Topical Review

# Topical Review: Development of overgrown semi-polar GaN for high efficiency green/yellow emission

T Wang

Department of Electronic and Electrical Engineering, University of Sheffield, Mappin Street, Sheffield S1 3JD, UK

E-mail: [t.wang@sheffield.ac.uk](mailto:t.wang@sheffield.ac.uk)

Received 14 August 2015, revised 26 May 2016

Accepted for publication 23 June 2016

Published 10 August 2016



CrossMark

## Abstract

The most successful example of large lattice-mismatched epitaxial growth of semiconductors is the growth of III-nitrides on sapphire, leading to the award of the Nobel Prize in 2014 and great success in developing InGaN-based blue emitters. However, the majority of achievements in the field of III-nitride optoelectronics are mainly limited to polar GaN grown on *c-plane* (0001) sapphire. This polar orientation poses a number of fundamental issues, such as reduced quantum efficiency, efficiency droop, green and yellow gap in wavelength coverage, etc. To date, it is still a great challenge to develop longer wavelength devices such as green and yellow emitters. One clear way forward would be to grow III-nitride device structures along a semi-/non-polar direction, in particular, a semi-polar orientation, which potentially leads to both enhanced indium incorporation into GaN and reduced quantum confined Stark effects. This review presents recent progress on developing semi-polar GaN overgrowth technologies on sapphire or Si substrates, the two kinds of major substrates which are cost-effective and thus industry-compatible, and also demonstrates the latest achievements on electrically injected InGaN emitters with long emission wavelengths up to and including amber on overgrown semi-polar GaN. Finally, this review presents a summary and outlook on further developments for semi-polar GaN based optoelectronics.

Keywords: semipolar GaN, overgrowth, InGaN, LED

(Some figures may appear in colour only in the online journal)

## 1. Introduction

The last two decades have seen major developments in III-nitride optoelectronics on sapphire substrates. This is a result of technological breakthroughs in the epitaxial growth of GaN on sapphire in spite of a 16% lattice mismatch and the achievement of both p-GaN and InGaN with great optical performance, due essentially to the pioneering work of Akasaki and Amano in the late 1980s [1, 2] and Nakamura in the early 1990s [3]. However, the great success in the field of III-nitride optoelectronics are mainly limited to InGaN-based blue emitters on polar GaN grown on a *c-plane* (0001)

sapphire. More recently, there have been some impressive results on the progress of green emitters, in spite of the difficulties in achieving emitters with an emission wavelength above 500 nm on *c-plane* GaN. For instance, 524 nm laser diodes (LDs) operating at room temperature in a continuous wave (CW) mode have been demonstrated [4] and 531 nm LDs operating at room temperature in a pulsed mode have also been reported [4]. However, both green LDs and green light emitting diodes (LEDs) on conventional *c-plane* GaN generally show inferior properties compared to their counterpart blue or violet LDs and LEDs. For longer wavelengths, such as yellow or even red, the progress is even slower;

research on InGaN-based yellow emitters has remained on the same level as before the year 2000 [5, 6]. These facts imply that there exist a number of fundamental challenges hampering the growth of longer wavelength emitters on *c-plane* GaN. It is also extremely difficult to employ other III-V semiconductors such as (Al,Ga,In)P to fabricate efficient emitters in the green and yellow spectral region [7], thus generating the so-called ‘Green/Yellow Gap’.

Longer wavelength emitters are not only important for the fabrication of solid-state lighting devices with ultra-high energy efficiency but also crucial for increasingly demanding opto-genetics applications [8], the emerging technology which combines optical and genetic methods in order to tackle diseases such as Parkinson’s disease.

The ultimate solid-state lighting source for general illumination would require a combination of different wavelength LEDs all with high efficiency as opposed to the current ‘blue LED + yellow phosphor’ approach. In this case, a mixture of at least either blue/yellow LEDs or blue/green/red LEDs is required. The lighting source fabricated in such a manner could potentially provide not only the highest efficiency but also the best colour rendering. Furthermore, the utilisation of discrete wavelength LEDs would also provide the best approach to tuning colour temperature in order to replicate the colour temperature of the Sun.

Visible light can be used as a genetically encoded switch to turn neurons on or off depending on the wavelength. For example, blue light at 470 nm can activate channelrhodopsin, while yellow light at 570 nm can activate halorhodopsin [8]. This property is being suggested for research on epilepsy or Parkinson’s disease, bringing new hope for patients who are suffering from vision impairment or neurological disorders.

One of the fundamental issues that prevents longer wavelength LEDs is the polar orientation of *c-plane* GaN, leading to strain-induced piezoelectric fields across InGaN/GaN quantum well structures as a result of the lattice-mismatch between InGaN and GaN. Consequently, InGaN-based emitters exhibit a reduced overlap between electron and hole wave-functions leading to long radiative recombination times and thus low quantum efficiency, the so-called Quantum Confined Stark Effect (QCSE). This becomes a severe issue for green emitters and even worse for yellow emitters as a much higher InN fraction is required in the InGaN active layer and thus the increased strain generates even stronger piezoelectric fields. The reported yellow and red emitters mentioned above were obtained by actually using the QCSE; a thick InGaN quantum well is used in order to enhance the redshift in emission wavelength as a result of the induced internal electrical fields [5, 6]. Of course, in this case, the quantum efficiency is greatly reduced.

Another fundamental limit is due to the so-called efficiency droop which occurs in all current InGaN based-LEDs on *c-plane* GaN, leading to a significant reduction in internal quantum efficiency (*IQE*) with increasing injection current [9, 10]. At the drive currents required for practical applications the *IQE* falls by up to 50% of its peak value, resulting in significant energy loss. This issue becomes more severe when the emission wavelength shifts towards the green/yellow

spectral region [9]. Although the mechanism for the efficiency droop is not yet fully understood, it is generally believed that the QCSE plays an important role [9].

In addition to the above, the unfavourable vapour pressure of indium over the compound requires a low growth temperature for InGaN and the higher the indium content, the lower the temperature. This has the potential to prevent defect-free epilayers required for longer wavelength emitters with high efficiency.

The QCSE issue also leads to a very limited bandwidth or modulation speed when utilising white LEDs as optical transmitters for wireless communications. An emerging technology called visible light communication (VLC) has a number of major advantages over the present-day radio frequency (RF) based WiFi technology [11]. Simply speaking, the maximum modulation speed or bandwidth is the inverse of carrier recombination lifetime ( $\tau$ ) within a LED, namely,  $f \sim 1/\tau$ . This carrier recombination lifetime can be expressed in terms of radiative and non-radiative carrier recombination lifetimes, labelled as  $\tau_{\text{rad}}$  and  $\tau_{\text{non-rad}}$ , respectively:

$$\tau^{-1} = \tau_{\text{rad}}^{-1} + \tau_{\text{non-rad}}^{-1}$$

The typical carrier recombination lifetime of current *c-plane* LEDs is  $\sim 10$  ns for blue and  $\sim 100$  ns for green, respectively, limiting the bandwidth to the order of MHz. Currently, an increase in bandwidth is obtained only through sacrificing the optical efficiency of the LEDs used, i.e., to enhance non-radiative carrier recombination by significantly increasing injection current density in order to generate the efficiency droop mentioned above, leading to a significant increase in the non-radiative carrier recombination rate and thus a reduction in total carrier recombination lifetime. Obviously, it is not an ideal solution.

One promising way forward to overcome the fundamental challenges discussed above is to grow InGaN/GaN hetero-structures along a semi- or non- polar direction which can effectively reduce or eliminate the internal electric fields. For example, the electric fields vanish completely if a crystal facet is perpendicular to the *c-plane*. Such facets include the (1120) and the (1010), also called the *a-plane* and *m-plane*, respectively. Crystal planes orientated between these two extremes (i.e., polar and non-polar) are called ‘semi-polar’ planes. In these cases, the internal fields are reduced depending on its inclination angle with respect to the *c-axis*, for example, (11-22) GaN is  $\sim 58^\circ$  with respect to the *c-axis*, whereas (20-21) is inclined at  $75^\circ$  to the *c-axis*. Figure 1 shows a summary of some typical semi-polar and non-polar planes in GaN [69] and figure 2 displays piezoelectric fields induced polarisation for InGaN with different indium compositions pseudomorphically grown on GaN as a function of the angle between the substrate normal and the *c-axis* [32].

The earliest work on semi- or non- polar GaN was mainly focused on calculation, reported by Takeuchi, Amano and Akasaki [12]. They calculated the longitudinal piezoelectric field and transition probability in a strained 3 nm InGaN/GaN quantum well structure as a function of the polar angle from the *c-axis*. Their calculation demonstrates that the highest

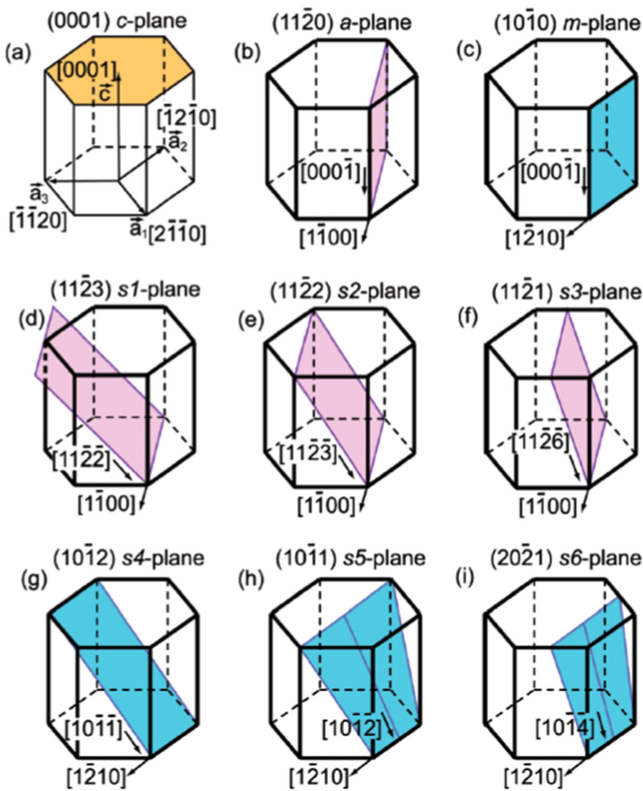


**Figure 1.** Schematics of crystallographical planes of some typical semi- or non-polar GaN. This figure is reproduced from [69], with the permission of AIP Publishing.

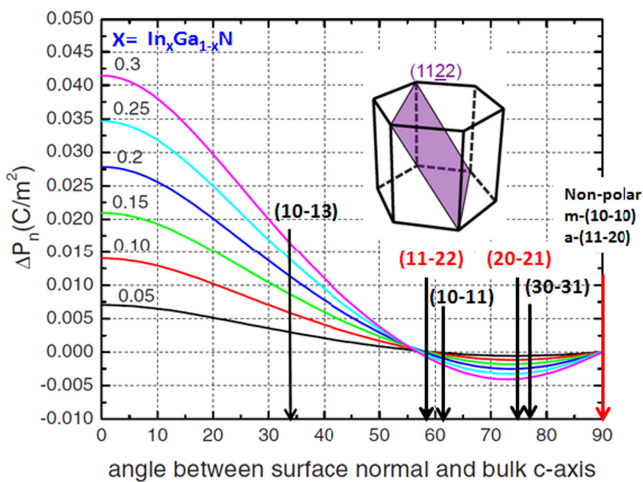


**Figure 2.** Polarisation of InGaN with different indium composition on GaN as a function of the angle between the substrate normal and the  $c$ -axis. This figure is modified and reproduced from [32], with the permission of AIP Publishing.

piezoelectric field is along the (0001) direction, resulting in the lowest transition probability which occurs in current III-nitride devices. However, the piezoelectric field is reduced to almost zero and the transition probability is significantly enhanced when the crystal facets are inclined from the (0001) direction, i.e., semi- or non-polar GaN.

McLaurin *et al* [13] reported a highly increased hole concentration in a p-type  $m$ -plane GaN layer up to

$7 \times 10^{18} \text{ cm}^{-2}$ , almost one order of magnitude higher than for (0001) GaN. Tsuchiya *et al* [14] reported a similar result on a p-type  $a$ -plane GaN layer and showed an activation energy of 118 meV for Mg acceptors, which is much lower than the 150–170 meV for current GaN layers grown along the polar (0001) direction. This may be the reason for the highly increased hole concentration in p-type  $a$ - or  $m$ -plane GaN. A first-principles calculation also shows that Mg atoms can be easily incorporated into electrically active substitutional lattice sites on the semi-polar (10-1-1) GaN surface [15]. Park [16] predicted that the effective hole mass in strained non-polar InGaN quantum wells should be smaller than that in strained  $c$ -plane InGaN quantum wells, which will potentially increase the hole mobility and then improve the conductivity of p-type semi- or non-polar GaN. Clearly these data indicate that semi- or non-polar GaN demonstrates great potential to be fabricated into optoelectronic devices with superior performance compared to  $c$ -plane GaN-based emitters.

The earliest attempt at the growth of semi- or non-polar GaN was reported by Sasaki *et al* [17] in 1986 just before Akasaki and Amano published their two-step growth method. They may not have paid much attention to whether it was semi- or non-polar or not, but rather were looking for the best oriented sapphire for the growth of GaN. Their conclusion was that the lattice mismatch between (0112) sapphire and the resultant epitaxial (2-1-10) GaN is smaller than that between the (0001) sapphire and the (0001) GaN. The first deliberate attempt at non-polar GaN growth was reported in 2000 [18]. In this case, the substrate was  $\text{LiAlO}_2$  and the deposition technique was molecular beam epitaxy (MBE). The growth of GaN on  $\text{LiAlO}_2$  substrates via the much more common technique of metalorganic vapour phase epitaxy (MOVPE) is difficult due to the high diffusivity of Li and Al atoms at the high temperature required for the growth of III-nitrides.

The great academic and commercial success achieved by the growth of  $c$ -plane GaN on (0001) sapphire and the potential gains to be had by looking at other orientations have encouraged scientists to study the growth of semi- or non-polar GaN on sapphire or Si. It has been found that semi- or non-polar GaN can indeed be obtained by growing GaN on  $r$ -plane or  $m$ -plane sapphire using the classic two-step growth approach. Conversely it has been found that it is extremely difficult to achieve semi- or non-polar GaN on any planar Si substrate [19]. Atomically flat surfaces have been achieved on  $r$ -plane or  $m$ -plane sapphire by means of the classic two-step approach or a high temperature AlN buffer method [33], but the crystal quality of the epi-layer is far from the requirements for the growth of any device structures; the full width at half maximum (FWHM) of x-ray diffraction rocking curves is typically  $0.2\text{--}0.3^\circ$  compared with just  $0.08^\circ$  for  $c$ -plane GaN on sapphire.

Unlike  $c$ -plane GaN grown on sapphire, another issue for semi- or non-polar GaN is the high density of stacking faults in addition to dislocations. In  $c$ -plane polar GaN, stacking faults are restricted to the interface between the GaN and sapphire and furthermore are perpendicular to the growth direction. Consequently, the stacking faults cannot extend to

the surface and thus there is no concern about the influence of stacking faults on device performance. However, the stacking fault planes are parallel to the growth direction in non-polar GaN, or inclined to the growth direction in semi-polar GaN. As a consequence, they can pass through all the upper layers and finally extend to the surface of any device structure. Both dislocations and stacking faults are supposed to affect both the electrical and optical performance of semi- or non-polar GaN-based optoelectronics.

Right now, we have understood that it would be impossible to achieve semi- or non-polar GaN with device quality directly grown on any planar non-*c-plane* foreign substrates, implying that the growth of *c-plane* GaN on (0001) sapphire (lowest index surface) would be a unique success for current GaN-based optoelectronics achieved on (0001) sapphire.

So far, all semi- or non-polar InGaN-based emitters with the best performance including blue/green LEDs are grown on free-standing semi-/non-polar GaN substrates [20–24]. These free-standing substrates are obtained by means of growing a polar *c-plane* GaN layer on sapphire to a thickness of up to 10 mm by a hydride vapour phase epitaxy (HVPE) technique and then slicing along a semi- or non-polar orientation [25–27]. As a result, these free-standing substrates are limited to a typical size of  $10 \times 10 \text{ mm}^2$  and are also extremely expensive. So far, by this method a few companies such as Mitsubishi Chemical Corporation (MCC) and Furukawa Company Ltd can provide free-standing semi- or non-polar GaN substrates. In addition to the HVPE techniques, an ammonothermal growth technique has been developed and has the potential to lead to GaN with larger dimensions, thus increasing the size of free-standing semi- or non-polar GaN substrates. Recently, AMMONO has reported their latest result of an *m-plane* GaN substrate with a diameter of 1 inch ( $26 \times 26 \text{ mm}^2$ ) using the ammonothermal growth technique. In spite of the extremely high price of free-standing semi- and non-polar GaN substrates, they have found some niche applications, such as the growth of laser structures. However, ultimately it is necessary to develop cost-effective semi- or non-polar GaN on  $\geq 2$  inch substrates in order to meet the industrial requirements for the growth of LED structures. To this end, a start-up company in the UK, Seren Photonics Ltd, has started to ship 2 inch semi-polar GaN templates on sapphire at a fraction of the cost of free-standing material.

This topical review starts by presenting the background to the development of semi-polar GaN and the major advantages of semi-polar GaN compared with *c-plane* GaN. The second section details a number of the challenges in the epitaxial growth of semi-polar GaN on foreign substrates and specifically highlights why overgrowth techniques are particularly suitable for the epitaxial growth of semi-polar GaN. A number of overgrowth techniques for semi-polar GaN on sapphire and on Si will be discussed. A detailed structural investigation of semi-polar GaN, including the mechanisms for defect reduction, will be provided based on x-ray and high resolution Transmission Electron Microscopy (TEM) measurements. As already mentioned, semi- and non-polar GaN also contains another kind of major defect, the Basal Stacking

Faults (BSFs) which are not an issue for *c-plane* material. A specific subsection will be devoted to the study of BSFs. A comparative study of the optical properties of InGaN quantum well structures on semi-polar GaN with their counterparts on *c-plane* GaN will be made, concentrating on the long wavelength spectral region. The review will also demonstrate the latest achievements on electrically injected InGaN emitters with long emission wavelengths (up to amber) on overgrown semi-polar GaN templates. Finally, the review will provide a summary and outlook on further developments for semi-polar GaN based optoelectronics.

## 2. Current status of development of semi-polar GaN

InGaN alloys have direct bandgaps across the entire composition range from 0.7 eV for InN to 3.43 eV for GaN, transcending the complete visible spectrum, part of the ultraviolet (UV) and part of the infrared. In theory, InGaN could replace most other III-V semiconductors in terms of bandgap range. To achieve long wavelength emission requires InGaN with high indium content, typically  $>20\%$ . Unfortunately, it is a great challenge to obtain InGaN with both high indium content and high optical performance on *c-plane* GaN. This is because the typical approach to obtaining high indium content is to lower the growth temperature, which is not ideal as it leads to a reduction in crystal quality. Another solution is to grow InGaN on a relaxed layer. It has been reported that stress can change the vapour-solid thermodynamic equilibrium, reducing the solid-phase epitaxial composition towards lattice-matched conditions and thus limiting indium incorporation into GaN [28–31]. Therefore, growth on a relaxed layer would help to increase indium content. However, a relaxed layer is normally formed at the expense of defects generated in hetero-structures [31], and thus, although this idea is currently used for the growth of contemporary green emitters on *c-plane* GaN, it is ultimately not an ideal solution.

In addition to the challenge in achieving high crystal quality as a result of the substrate issue, the formation mechanism of InGaN alloys is complicated, in particular, for high indium content InGaN. The In-N bond is  $\sim 11\%$  longer than the Ga-N bond, leading to a strained repulsive interaction between incorporated indium atoms on a surface. Northrup's first-principles calculation demonstrates that indium chemical potential required for the incorporation of indium atoms depends on surface structure [32]. On a semi-polar GaN surface, such as (11-22), the incorporated indium atoms have lower repulsive interaction than those on non-polar or polar surfaces and thus the incorporation of indium atoms can be obtained at a significantly lower indium chemical potential than is required for the incorporation of indium on either non-polar or polar surfaces. It means that semi-polar GaN surfaces can accommodate more indium atoms than either non-polar or polar surfaces, leading to more favourable growth of InGaN with high indium content than that on either non-polar or polar surfaces. This also implies that the growth of InGaN with high indium content could be potentially performed at a

**Table 1.** Inclination angle of semi-polar GaN with respect to *c-plane* GaN.

Semi-polar GaN	Angle to <i>c-plane</i> GaN	Planar substrates	Patterned substrates
(10-11)	62	(100) spinel [36]; (30-38) 4H-SiC [35];	(001) Si [37, 38]; (11-23) sapphire [39];
(10-12)	43	(001) Si with 2°–6° off-axis [40];	No report
(10-13)	32	(110) spinel [36]; <i>m-plane</i> sapphire [41–43];	No report
(10-15)	18	(001) Si [44];	No report
(10-16)	26	(113) Si [45];	No report
(11-22)	58	(112) Si [40]; <i>m-plane</i> sapphire;	<i>r-plane</i> sapphire [47–53]; (113) Si [54–56];
(20-21)	75	No report	(22–43) sapphire [57, 58]; (114) Si with 1° off-axis [59];
(30-3-1)	80	No report	No report

relatively high temperature on semi-polar GaN which is helpful for improving the crystal quality of the InGaN.

Comparing indium incorporation on non-polar and polar GaN surfaces, it has been reported that indium incorporation efficiency on a non-polar surface is 2 or 3 times less than that on a *c-plane* polar GaN [31].

Clearly, it would be more favourable to grow long wavelength emitters on a semi-polar GaN surface than on any other orientation. To date, a number of semi-polar GaN planes with a wide range of inclination angles to the *c-plane* GaN have been reported upon.

Table 1 summarises all the planar or patterned substrates on which semi-polar GaN has been directly grown to date. Although a number of semi-polar GaN planes have been reported, only a few kinds of semi-polar GaN can be directly grown on planar substrates such as sapphire, which is commercially available and industry compatible. (11-22) or (10-13) GaN can be directly grown on planar *m-plane* sapphire substrates, depending on the nitridation conditions [34]. A high temperature sapphire nitridation process generally leads to the formation of (10-13) GaN, while a low temperature nitridation process favours the growth of (11-22) GaN. (10-13) GaN grown on sapphire typically suffers from intrinsic surface problems, such as the formation of micro-twinning structures during the growth which may not be good for further growth of device structures, while (11-22) GaN shows a smooth surface.

In 2005, the team at Meiji University reported (10-11) GaN directly grown on planar (30-38) 4H-SiC substrates [35]. However, since then no further progress has been reported, possibly implying major challenges which cannot be resolved. Baker *et al* [36] reported (10-1-1) and (10-1-3) semi-polar GaN directly grown on different kinds of planar spinel (MgAl<sub>2</sub>O<sub>4</sub>) substrates, namely, (10-1-1) semi-polar GaN on (100) spinel and (10-1-3) semi-polar GaN on (110) spinel, respectively.

It is difficult to grow semi-polar GaN on any planar Si substrate, in particular, the growth of semi-polar GaN with a high inclination angle to *c-plane* for which Si substrates with a high index are required as shown in table 2 [19]. It is well-

known that the growth on high index Si substrates generally poses great challenges in achieving high crystal quality.

Some semi-polar GaN on foreign substrates can be achieved only through growth on patterned substrates, for example, (20-21) semi-polar GaN. (20-21) semi-polar GaN is obtained predominately by growth of a very thick *c-plane* GaN by the HVPE technique and then slicing it along the orientation as discussed above. However, recently, there are a few reports on the growth of (20-21) semi-polar GaN on patterned (22-43) sapphire [57, 58] or patterned (114) Si cut at 1° off-axis [59]; although in both cases the research is in its infancy and thus they also suffer from a number of growth difficulties including surface morphology. For the former the major disadvantage would be the great challenges in fabricating patterned (22–43) sapphire with a specific groove angle which can meet the requirements to achieve (20-21) GaN by selective growth.

Currently (30-3-1) semi-polar GaN is only available in the form of free standing and small substrates obtained by slicing a thick HVPE *c-plane* GaN layer grown on sapphire [60].

### 2.1. Indium incorporation into GaN on semi-polar GaN surfaces

It has been accepted that the inclination angle to the *c-plane* GaN would have to be around 45°–60° or higher in order to maximise the advantages of semi-polar GaN in terms of optical performance. Overall, it has been understood that (11-22) GaN and (20-21) GaN are the two most promising planes among the various semi-polar planes used as the substrates for the growth of semi-polar GaN LEDs and LDs. (11-22) GaN and (20-21) GaN have different advantages and can be used for the growth of optoelectronics with different applications.

A systematic study of indium incorporation into GaN as a function of semi-polar GaN planes has been performed by Wernicke *et al* [61] who have investigated the optical performance of a number of InGaN/GaN multiple quantum well (MQW) structures on various free-standing semi-polar GaN substrates, namely, (10-11), (10-12), (11-22) and (20-21). The results have been compared with the InGaN/GaN MQWs

grown on *c-plane* GaN substrates, demonstrating that an indium incorporation as a function of semi-polar GaN planes can be described as [61]:

$$(10-11) > (11-22) > (0001) = (20-21) = (10-12)$$

Through a wide range of growth temperatures, indium incorporation on both (10-11) GaN and (11-22) GaN are significantly enhanced compared with those on the *c-plane* GaN, while other semi-polar GaN planes including (20-21) are not particularly good for enhancing indium incorporation. Consequently, this makes both (10-11) GaN and (11-22) GaN extremely important for the growth of longer wavelength such as green and yellow emitters in order to overcome the green/yellow gap. However, (10-11) GaN suffers from a surface morphology issue naturally forming hillocks during its epitaxial growth [27], while there is no such a problem for (11-22) GaN. So far, it is unclear whether the surface issue of (10-11) GaN is due to intrinsic problems or growth techniques used. Overall, this currently leaves only one option for the growth of longer wavelength emitters in terms of semi-polar GaN orientation; (11-22) GaN.

Further evidence has been provided by Zhao *et al* [62]. They performed a systematic study on comparing the indium incorporation rate on different semi-polar GaN surfaces, (11-22), (20-21), and (30-3-1), showing different emission wavelengths of InGaN quantum well structures grown under identical conditions as displayed in figure 3. Throughout a wide range of growth conditions (11-22) GaN leads to longest emission wavelength. For example, the LEDs grown on the (20-2-1) GaN and the (20-21) GaN show 470 nm and 438 nm emission, respectively, while the LEDs grown on the (11-22) GaN leads to 490 nm emission. The shortest wavelength is from the LEDs grown on the (30-3-1) GaN. This further strengthens the advantages of using (11-22) GaN for the growth of longer wavelength emitters.

Generally speaking, it has been widely recognised that nitrogen-polar GaN has to be avoided due to a number of disadvantages, such as severe surface issues, chemical instability, etc. However, the nitrogen-polar orientation of GaN also exhibits two major advantages in terms of enhanced indium incorporation efficiency and reduced QCSE. In the case of Ga-polar GaN, indium species only weakly interact with indium and gallium surface atoms and thus the growth of high indium content layers generally requires a low growth temperature. In contrast, nitrogen surface atoms lead to the formation of stronger In-N bond in the case of nitrogen-polar GaN and as a result high indium content can be possibly achieved at an elevated growth temperature. Another advantage is due to the reverse direction of the polarization in nitrogen-polar InGaN compared with Ga (or In)-polar InGaN. As a consequence, a nitrogen-polar device potentially leads to reduced QCSE across the InGaN quantum wells during an electrical operation, while a Ga-polar emitter requests an increase in forward bias voltage, increasing the electric field across the InGaN quantum wells and further enhancing the QCSE. This would become more distinguished for InGaN emitters with longer emission wavelength. So far,

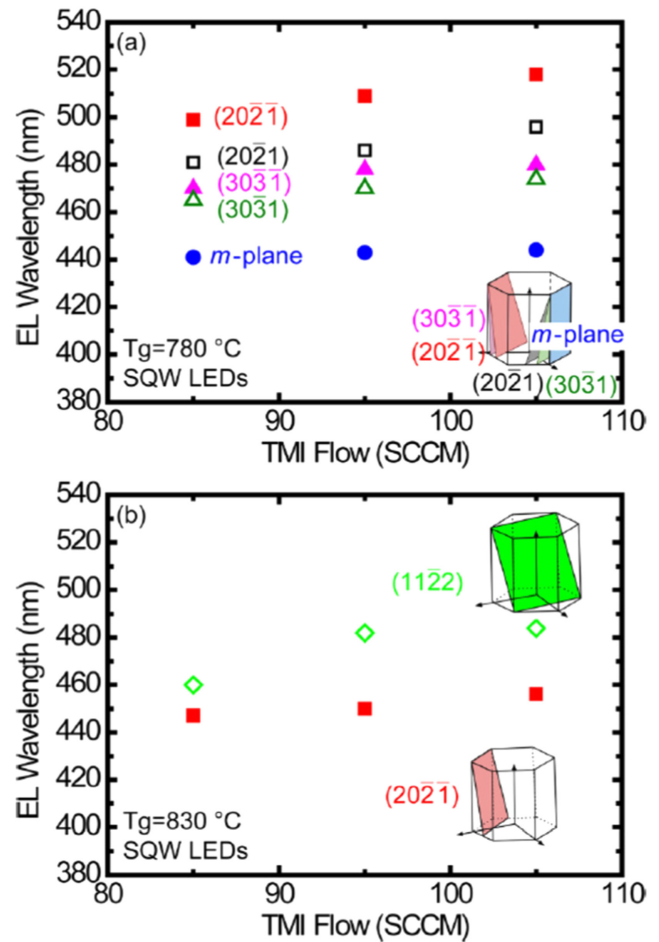


**Figure 3.** Electro-luminescence emission peaks of InGaN-based LEDs as a function of TMI In (Indium precursor) flow rate grown on different semi-polar GaN surfaces. This figure is reproduced from [62], with the permission of AIP Publishing.

unfortunately, there are a very limited number of reports [108, 109], although nitrogen green LEDs with an emission wavelength of 540 nm were demonstrated in 2011 [109]. Since then, there are no further reports, implying that great challenges in growth would need to be overcome.

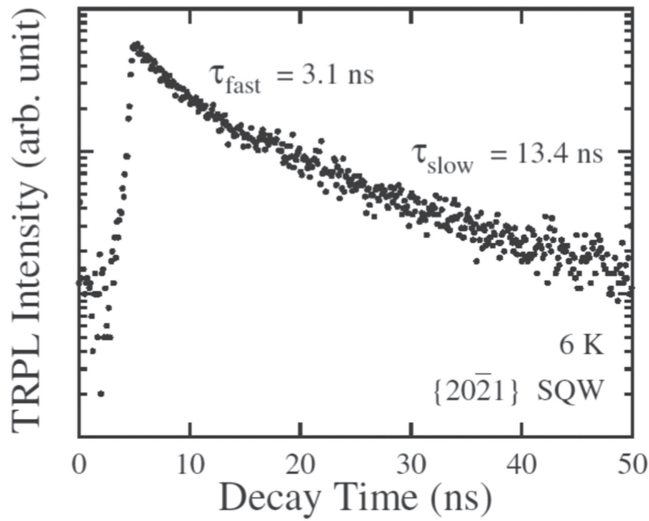
## 2.2. Excitonic dynamic properties of InGaN MQWs on different semi-polar GaN surfaces

A few teams have performed an excitonic dynamic study of InGaN quantum well structures grown on different semi-polar GaN surfaces, typically, (20-21) and (11-22), showing a significant difference between them. Such a study would be extremely important for practical applications such as VLC, as the maximum modulation speed or bandwidth is the inverse of the carrier recombination lifetime ( $\tau$ ) of LEDs.

Funato *et al* [63] performed time-resolved photoluminescence (TRPL) measurements on an InGaN single quantum well (SQW) structure with an emission wavelength of around 530 nm grown on semi-polar (20-21) GaN substrates with a threading dislocation (TD) density of  $< 1 \times 10^6 \text{ cm}^{-2}$ ; such a low dislocation density could exclude any influence of dislocations on optical properties. The

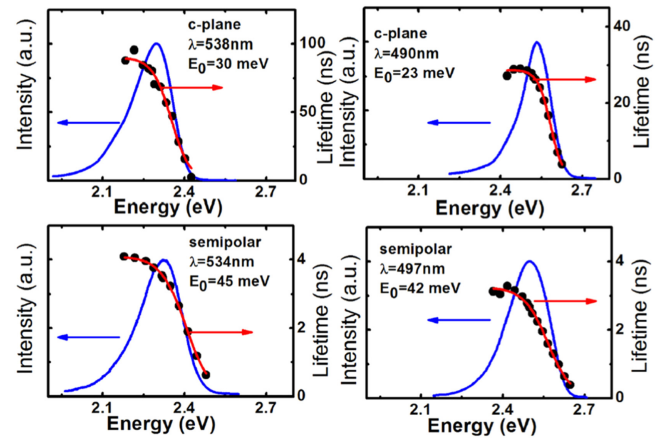
**Table 2.** *c*-axis tilt angle of GaN with respect to the surface normal [19].

(11 h)	(111)	(112)	(113)	(114)	(115)	(116)	(117)
<i>c</i> -axis title angle (deg)	0	18	26	29	31	34	47

**Figure 4.** TRPL decay trace of (20-21) InGaN SQW measured at 6 K [63]. Copyright 2010 The Japan Society of Applied Physics.

sample structure used consists of a 2  $\mu\text{m}$  thick n-type GaN buffer layer directly grown on the GaN substrates, a 100 nm thick undoped InGaN pre-layer with low indium content and finally an InGaN SQW where a 3 nm InGaN quantum well is sandwiched between a 15 nm undoped GaN barrier and 10 nm undoped GaN capping layer. Figure 4 shows the PL decay curve of the InGaN SQW structure measured at 6 K. From figure 4, a radiative recombination lifetime of 3.1 ns has been obtained and is much shorter than a typical radiative recombination lifetime of  $\sim 85.0$  ns for a green InGaN MQW structure grown on *c*-plane GaN, demonstrating a significant reduction in piezoelectric fields on the (20-21) plane.

A team at the University of Sheffield has performed TRPL measurements on green InGaN MQW structures grown on their overgrown (11-22) GaN templates with significantly improved crystal quality, achieved by using a self-organised nickel nano mask approach [64]. The sample consists of three-period 3 nm InGaN MQWs with an emission wavelength of  $\sim 530$  nm, similar to the above (20-21) SQW structure. The TRPL measurements were performed at 77 K, showing a radiative recombination lifetime of less than 1 ns. This is significantly shorter than that of the (20-21) SQW structure with a similar emission wavelength. This implies that the (11-22) GaN is more favourable for the fabrication of LEDs for the VLC applications than (20-21) GaN. Very similar results have also been reported by Kawakami's group [65], although they performed TRPL measurements on an InGaN quantum well structure with lower indium composition (428 nm) grown on (11-22) GaN substrates, measured at 10 K. They reported a radiative recombination lifetime (fast decay component) of only 46 ps. This would be excellent for

**Figure 5.** PL decay time as a function of emission energy for two polar (0001) and two semi-polar (11-2 2) InGaN/GaN MQW samples with different emission wavelengths measured at 7 K. The red lines are the fitting results. This figure is reproduced from [64], with the permission of AIP Publishing.

the fabrication of LEDs for VLC applications, potentially leading to modulation speeds of up to 20 GHz.

Previously we have understood that the large immiscibility between GaN and InN leads to phase separation induced indium fluctuation in InGaN alloys when the indium content exceeds 6% [66]. This is expected to become more severe in InGaN alloys with higher indium content required for the growth of green or yellow emitters. The indium fluctuation induced localisation effect has been accepted to play an important role in preventing carrier diffusion to non-radiative centres, thus leading to enhanced optical efficiency even though a high density of dislocations exist in *c*-plane GaN grown on sapphire. This is one of the keys to achieving great success with blue LEDs. However, the inhomogeneity also has some negative influence on the optical properties of InGaN-based optoelectronics due to disturbing uniform population inversion, leading to an increase in the threshold current of LDs.

The carrier localization of InGaN quantum well structures can be studied by using wavelength-dependent TRPL measurements [67]. The carrier recombination lifetime decreases with increasing detection energy, indicating the existence of localized excitons in exponential-tail density of states [67]. This can be described by:

$$\tau = \tau_{\text{rad}} \left/ \left[ 1 + \exp\left(\frac{E - E_m}{E_0}\right) \right] \right.$$

where  $\tau_{\text{rad}}$  and  $E_m$  are the radiative lifetime and the energy of the mobility edge respectively;  $E_0$  represents the exciton localization depth.

Figure 5 presents the fast decay lifetime as a function of the monitored photon energy of a green and another dark blue

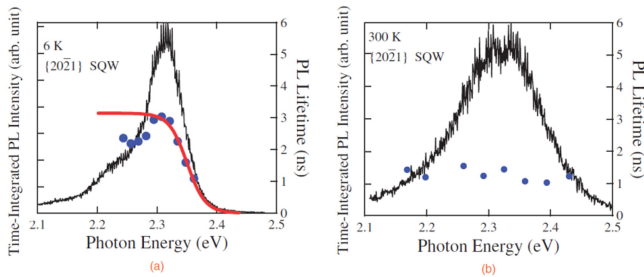


**Figure 6.** PL spectra and energy dependence of the PL lifetime, measured at 6 K (a) and 300 K (b) [63]. Copyright 2010 The Japan Society of Applied Physics.

InGaN MQW samples on (11-22) GaN templates measured at 7 K. Two *c-plane* samples with similar emission wavelengths are used for reference. The obtained localization depths are 30 meV and 23 meV for the *c-plane* green sample with an emission wavelength of 538 nm and the *c-plane* blue sample with an emission wavelength 490 nm, respectively, while the localization depths are 45 meV for the 534 nm green semi-polar sample, and 42 meV for the 497 nm blueish semi-polar sample, respectively. This indicates that (11-22) semi-polar GaN leads to enhanced indium fluctuation compared with *c-plane* GaN.

Funato *et al* [63] studied the exciton localization of a green InGaN quantum well structure grown on (20-21) GaN. Figure 6 shows the PL spectra and energy dependence of the PL lifetime, measured at 6 and 300 K respectively. Once again,  $E_0$  has been obtained and is 15.1 meV, which is much smaller than that of the green InGaN MQWs on *c-plane* GaN. Furthermore, the PL lifetime starts to decrease at  $\sim 150$  K ( $\sim 13$  meV) and then disappears at RT as shown in figure 6(b), indicating that the carriers/excitons are delocalised from the localization states with a depth of 15 meV. These data demonstrate that higher homogeneity of indium composition can be achieved on a (20-21) GaN surface even in the green region than that on the other planes. This has been further supported by measuring the FWHM of the electro-luminescence (EL) spectra of InGaN quantum well based LEDs grown on different GaN surfaces as shown in figure 7. From this figure it is clear that the LEDs grown on (20-21) GaN have narrower FWHM of EL spectrum than the LEDs grown on (11-22) GaN throughout a wide range of emission wavelengths [68].

In a general sense, (20-21) GaN demonstrates great potential to achieve laser diodes with a low threshold in terms of indium homogeneity. However, in terms of indium incorporation efficiency, it seems that (20-21) GaN does not show more advantages compared with *c-plane* GaN as discussed in section 2.1. The longest lasing wavelength, which is 531 nm, has been achieved on both (20-21) GaN and *c-plane* GaN substrates both operating only in a pulsed mode [4, 21]. Furthermore, the threshold current density for lasing in both cases are very similar. The threshold current densities of the 531 nm green LD on *c-plane* (0001) GaN substrates and (20-21) GaN substrates are  $18 \text{ KA cm}^{-2}$  and  $15.4 \text{ KA cm}^{-2}$ , respectively. However, there is a significant difference in wall

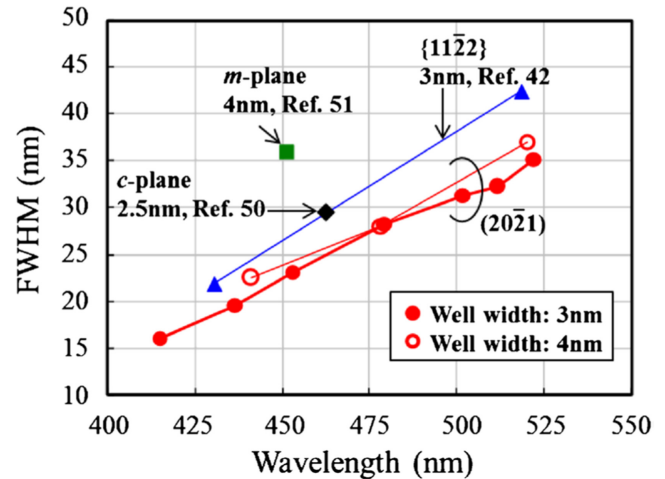


**Figure 7.** FWHM of the EL spectra of InGaN LEDs grown on different GaN surfaces throughout a wide range of emission wavelengths [68]. Copyright 2014 The Japan Society of Applied Physics.

plug efficiency of the green LDs grown on (20-21) GaN and *c-plane* GaN. Typically, the green LDs with an emission wavelength range from 525 to 532 nm grown on (20-21) GaN show wall plug efficiencies of 7.0%–8.9%, which are much higher than 2%–3% for *c-plane* LDs with similar wavelengths. Of course, due to the higher wall plug efficiency the green LDs grown on (20-21) GaN exhibit longer lifetimes than those grown on *c-plane* GaN.

The above data demonstrate that (20-21) GaN is an alternative and better option for developing green LDs, but does not show any major advantages in terms of developing even longer wavelength LDs such as yellow or amber. In this case, the only option is (11-22) GaN, although considerable effort needs to be devoted in terms of developing growth techniques.

In order to reduce the composition fluctuations, a more appropriate design of an InGaN quantum well and an improvement in growth techniques on (11-22) GaN are needed, such as tuning quantum well thickness using InGaN as a barrier, etc.

### 2.3. Other issues on (11-22) GaN and (20-21) GaN

There are some other issues relating to (11-22) GaN and (20-21) GaN, e.g. in both cases the basal plane is inclined with respect to the growth direction, leading to considerably large resolved shear stress on the basal (0001) plane in the growth of hetero-structures such as InGaN/GaN or AlGaIn/GaN quantum well structures as a result of their lattice-mismatch. This will be expected to generate misfit dislocations.

Romanov *et al* [69] calculated a shear stress as a function of the inclination angle of semi-polar GaN for two cases; InGaIn on GaN and AlGaIn on GaN. This is depicted in figure 8. The calculation performed is based on a misfit parameter, which in return depends on the inclination angle. Figure 8 indicates that the highest resolved shear stress occurs to (10-12) GaN, for which the inclination angle is  $43^\circ$ . The

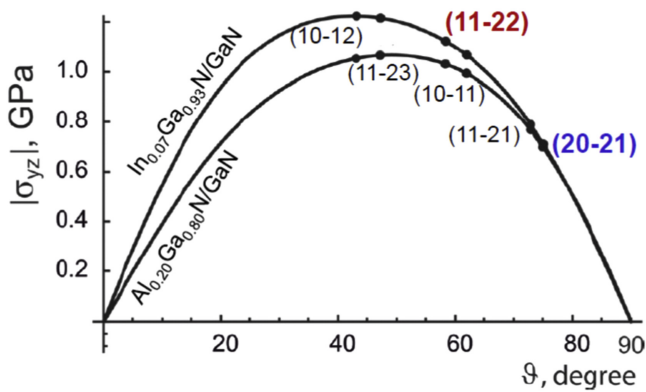


**Figure 8.** Shear stress of InGaN or AlGaIn on the GaN surface as a function of the angle between substrate normal and the  $c$ -axis. This figure is reproduced from [69], with the permission of AIP Publishing.

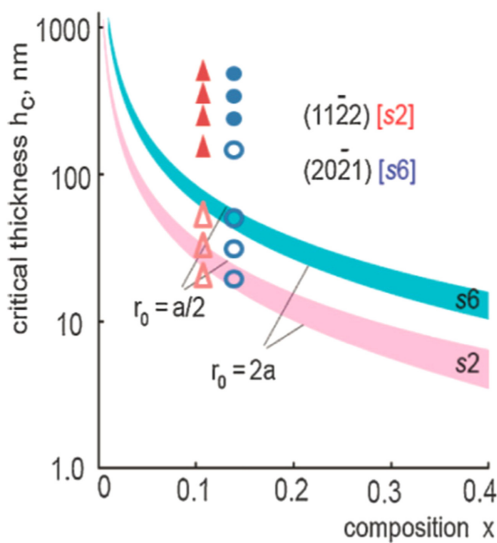


**Figure 9.** Critical thickness of InGaN or AlGaIn on a (11-22) and (20-21) GaN surface as a function of alloy composition [70]. Copyright 2010 The Japan Society of Applied Physics.

resolved shear stress for (11-22) GaN is larger than that for (20-21) GaN. Correspondingly, the critical thicknesses labelled as  $h_c$  for stress relaxation via the formation of misfit dislocation is expected to be different, also depending on the inclination angle. Larger resolved shear stress generally leads to a thinner critical thickness. This has been confirmed experimentally and theoretically by Yong *et al* [70]. Figure 9 shows a thinner critical thickness of either InGaN or AlGaIn grown on (11-22) GaN than those grown on (20-21) GaN. Therefore, we need to pay attention when designing InGaN MQWs grown on (11-22) or (20-21) GaN in order to eliminate the formation of misfit dislocations. In order to increase the critical thickness, an InGaIn buffer layer with low indium content or  $\text{In}_x\text{Ga}_{1-x}\text{N}$ : well/ $\text{In}_y\text{Ga}_{1-y}\text{N}$ : barrier would be necessary.

In addition to the above issues discussed in sections 2.1 and 2.2, very recent and detailed studies based on TEM indicate that there exists atomic-scale nano-facets at the interface of InGaIn quantum wells and GaN barriers grown on

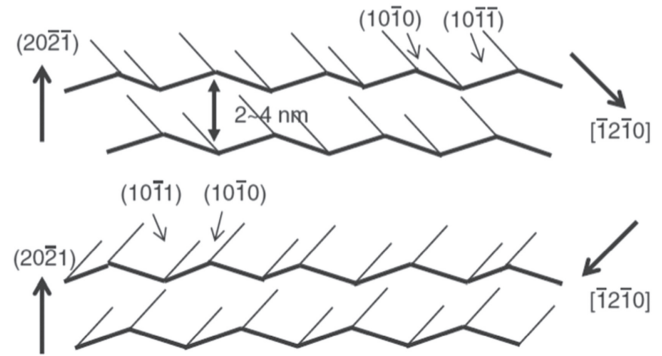


**Figure 10.** Schematic illustration of nano-facets appearing during the growth of InGaIn quantum wells on (20-21) GaN. Reproduced with permission from Elsevier [71].

(20-21) GaN [71, 72]. These nano-facets mainly consist of (10-10), (10-1-1) and (10-11) facets as schematically illustrated in figure 10. These nano-facets lead to significant fluctuations in quantum well thickness and the dimensionality of excitons. As a result, the carrier distribution and recombination process will be affected, including a large wavelength shift and a broadened spectral linewidth. So far, there is no report of such a phenomenon on (11-22) GaN, which gives another advantage compared with (20-21) GaN.

Overall, in terms of the growth of longer wavelength devices such as yellow or even red emitters including both LEDs and LDs, (11-22) GaN would be the most promising candidate, although a number of great challenges still exist, which could be potentially resolved through improving growth techniques and structure design. Furthermore, (11-22) GaN can be grown directly on planar sapphire, which is a great advantage to the commercial adoption of this technology.

### 3. Selective overgrowth of semi-polar GaN on sapphire and Si

Generally speaking, the (11-22) semi-polar GaN directly grown on planar sapphire substrates exhibits both a high density of dislocations and a high density of BSFs, typically  $>10^{10} \text{ cm}^{-2}$  and between  $10^5 \text{ cm}^{-1}$ – $10^7 \text{ cm}^{-1}$ , respectively. On the other hand, it would be impractical to use tiny and very expensive free-standing GaN as substrates, in particular, for the growth of LEDs. The growth of semi-polar GaN derived LEDs has to be based on sapphire or Si substrates if it is to be commercially attractive. Therefore, a cost-effective growth technology which would be accepted by industry is essential.

From the point of view of fundamental epitaxial growth, it would be favourable to perform growth on low index surfaces, as it potentially leads to high crystal quality. As already discussed, it is extremely difficult to obtain high crystal quality semi-polar (11-22) GaN grown directly on standard  $m$ -plane sapphire. However, if it were possible to grow (11-22) GaN on an inclined or tilted (0001) surface in order to make the in-plane with  $\sim 58^\circ$  to the  $c$ -axis, the epitaxial

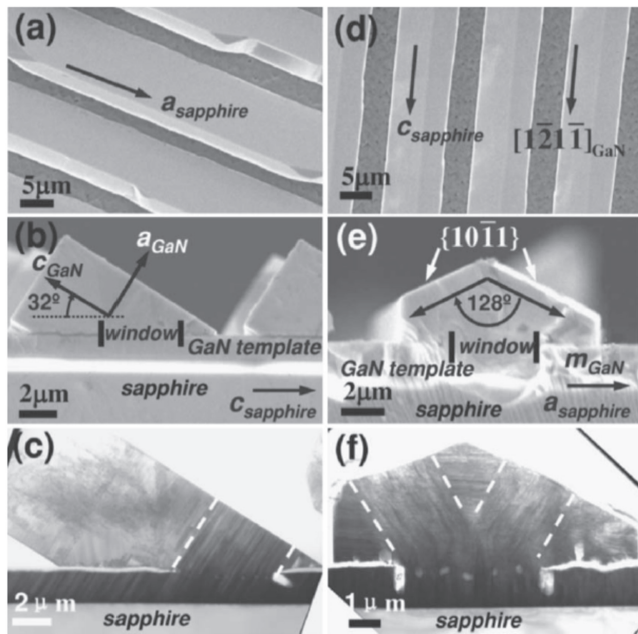


**Figure 11.** Plane and cross-sectional SEM images and cross-sectional TEM images of the ELOG samples with SiO<sub>2</sub> stripes oriented along the [1-210] *a*-axis (a), (b), (c), and the [0001] *c*-axis (e), (d), (f). This figure is reproduced from [73], with the permission of AIP Publishing.

growth would become straightforward as we are very familiar with *c*-plane GaN growth. Consequently, we might expect that the crystal quality of (11-22) GaN grown in such a way would be equivalent to that of its *c*-plane counterpart. Simply speaking, this is a kind of lateral epitaxial growth. Therefore, such lateral epitaxial growth is a favoured mode for the growth of any semi-polar or non-polar GaN, including epitaxial lateral overgrowth (ELOG) and lateral epitaxial growth on patterned substrates.

### 3.1. Conventional ELOG of semi-polar GaN

ELOG techniques have been developed for some time and have been successfully applied in the growth of *c*-plane GaN on sapphire, leading to a significant improvement in crystal quality. This has led to great success in achieving InGaN-based blue LDs. Of course, the ELOG techniques can also be applied in the growth of semi-polar GaN. Ni *et al* [73] reported ELOG of (11-22) semi-polar GaN on *m*-plane sapphire using an identical approach to that for the ELOG of *c*-plane GaN. A thin SiO<sub>2</sub> layer was initially deposited on a standard (11-22) semi-polar GaN template directly grown on *m*-plane sapphire. The standard semi-polar GaN template can be obtained using the classical two-step growth method and thus it shows a very broad x-ray rocking curve, indicating a high density of defects as expected. A standard lithography technique was then used to transfer a stripe mask pattern on the surface of the GaN template in order to form 10 μm SiO<sub>2</sub> stripes with 4 μm windows. Two orientations of SiO<sub>2</sub> stripes have been employed in order to make a comparison; one along the [1-210] *a*-axis and another along the [0001] *c*-axis

of the sapphire substrate. Figure 11 shows the plane and cross-sectional Scanning Electron Microscopy (SEM) images, and cross-sectional TEM images of these two ELOG samples, demonstrating that significant differences exist between them. Figure 11(b) shows that the ELOG technique leads to the formation of *c*-plane and *a*-plane GaN facets. The *c*-plane GaN facet clearly exhibits an inclination angle of 32° with respect to the substrate surface. Furthermore, figure 11(b) also confirms that the growth rate of *c*-plane GaN is much faster than that in other directions, leading to the growth of the *c*-plane GaN extending over the SiO<sub>2</sub> masks, while the lateral growth rate of the *a*-plane GaN is very slow. The TEM image in figure 11(c) indicates that both the dislocation density and the BSF density are significantly reduced in the wing-regions as a result of growth of the *c*-plane GaN extending over the SiO<sub>2</sub> masks. In the window regions, as expected both the dislocations and the BSFs penetrate from the semi-polar GaN template to the overlying layers. For the SiO<sub>2</sub> mask stripes oriented along the *c*-axis of the sapphire substrate, the lateral overgrowth should progress along the *m*-axis of GaN. The growth rate along the *m*-axis is very slow. Consequently, it would not be helpful for blocking the penetration of defects. Furthermore, figure 11(e) indicates that the growth along the *m*-axis leads to the formation of two {10-11} planes each inclining 26° to the substrate plane. The TEM study as shown in figure 11(f) indicates that neither dislocations nor BSFs can be blocked effectively.

Very recently, Song *et al* [74] employed the same ELOG technique to study the growth of semi-polar (11-22) GaN as a function of the SiO<sub>2</sub> stripe width of up to 12 μm. Similarly, they used a three-step procedure for their ELOG. The first step aims to form the seed GaN layer in the window regions, the second step is to enhance coalescence and the final step is to planarize the material.

For each of the different steps, the growth pressure and V/III ratio used are different. In order to achieve a coalesced and smooth surface, their overgrown layers were very thick, around 10 μm. Some impressive results have been achieved, showing that the crystal quality depends on the stripe width. Figure 12 displays the FWHM of x-ray diffraction (XRD) rocking curves measured along two typical directions, [-1-123] and [1-100], as a function of stripe width. When the stripe width increases from 6 to 10 μm, the FWHMs show a significant reduction. Any further increase in stripe width beyond 10 μm is not helpful for further improvement in crystal quality. However, it is worth highlighting that an increase in stripe width leads to challenges in coalescence and thus surface roughness issues. Figure 13 displays surface roughness as a function of stripe width, indicating that the surface roughness significantly increases with increasing stripe width. Atomic Force Microscopy (AFM) measurements as shown in the inset of figure 13 indicate that the roughness is clearly different between wing regions and window regions.

The ELOG technique has an intrinsic non-uniformity issue in both surface morphology and crystal quality and consequently optical property. The PL measurements show a massive difference between wing regions and window

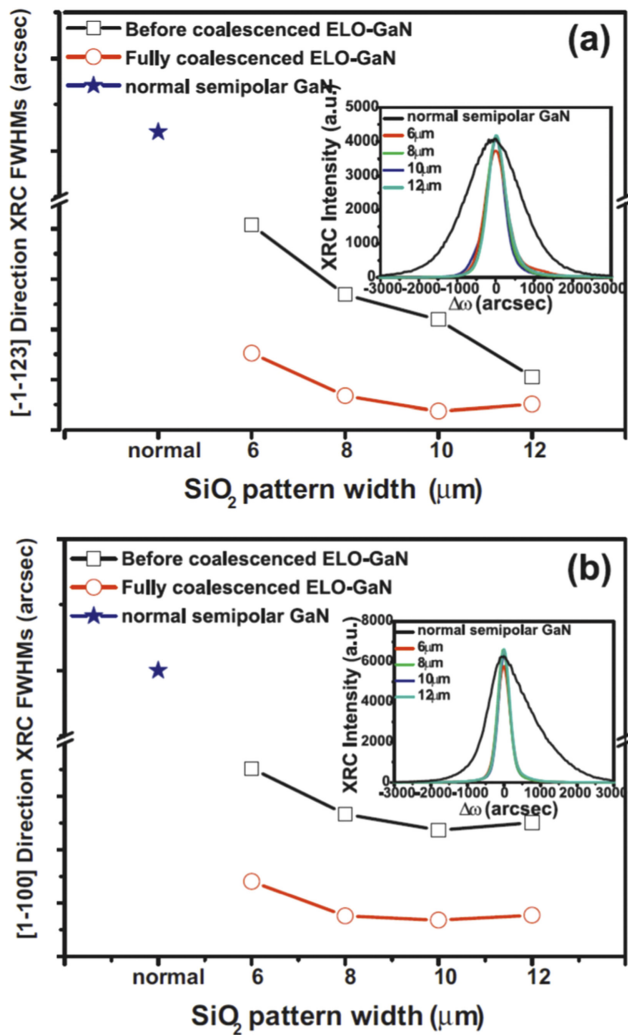


**Figure 12.** FWHM of x-ray rocking curves measured along two typical directions, [-1-123] and [1-100], as a function of stripe width. Reproduced with permission from Elsevier [74].

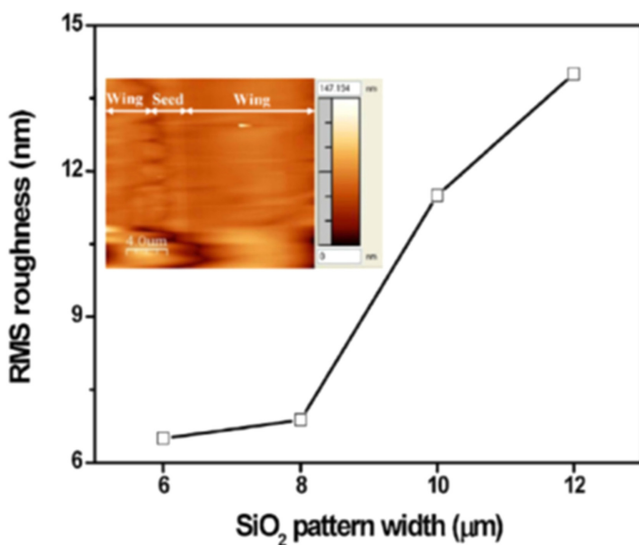


**Figure 13.** Surface roughness of ELOG GaN as a function of stripe width; and inset: AFM image (reproduced with permission from Elsevier [74]).

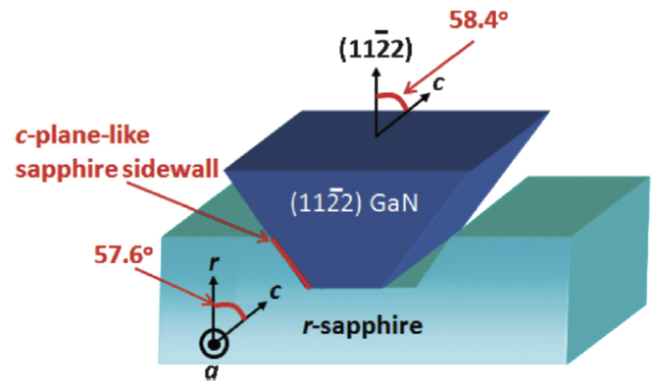


**Figure 14.** Schematic of patterned *r*-plane sapphire for growth of (11-22) GaN [50]. Copyright 2009 The Japan Society of Applied Physics.

regions, typically two-orders of magnitude higher PL intensity in the wing region than in the window regions.

### 3.2. Selective growth on patterned substrates

As discussed in the introduction of section 2, it would make the growth of semi-polar (11-22) GaN easy if we could manage to perform such growth on an inclined (0001) surface, while the (0001) surface has to incline with an angle of  $\sim 58^\circ$  to the substrate surface. Okada *et al* [50] proposed to grow semi-polar (11-22) GaN on patterned *r*-plane sapphire, as schematically illustrated in figure 14.

For *r*-plane sapphire, the angle between the *c*-axis and the *r*-axis is  $57.6^\circ$ , which is very close to  $58.4^\circ$ , the angle between the GaN (11-22) plane and the GaN *c*-plane. Therefore, (11-22) GaN can be formed along the vertical direction if the GaN growth takes place only on the *c*-plane surface of the *r*-plane sapphire as shown in figure 14. In this case, the key issue is to achieve a special grooved pattern with the particular inclination angle, where the *c*-plane-like sapphire sidewalls can be formed and then the GaN can be grown on the *c*-plane-like sapphire sidewalls. In principal, it is equivalent to the growth of *c*-plane GaN on (0001) sapphire surface, which inclines to the vertical direction by  $57.6^\circ$ .

Such *r*-plane sapphire with regularly grooved patterns can be fabricated by combining standard photolithography and dry-etching techniques using inductively coupled plasma (ICP) or reactive ion etching (RIE). The semi-polar (11-22) GaN can be obtained by performing growth on such patterned *r*-plane sapphire using the classic two-step growth method, i.e., a thin low temperature (LT) nucleation layer followed by a high temperature annealing process and then high temperature growth. Careful optimisation of growth conditions is required in order to avoid growth occurring on both *c*-plane sapphire sidewalls and *r*-plane surface. High temperature, high pressure and low V/III ratio are favourable for growth on the *c*-plane sapphire sidewalls.

The high temperature annealing process after the deposition of the LT nucleation layer makes the thin nucleation layer predominantly cover the *c*-plane-like sapphire sidewalls. This high temperature annealing process also

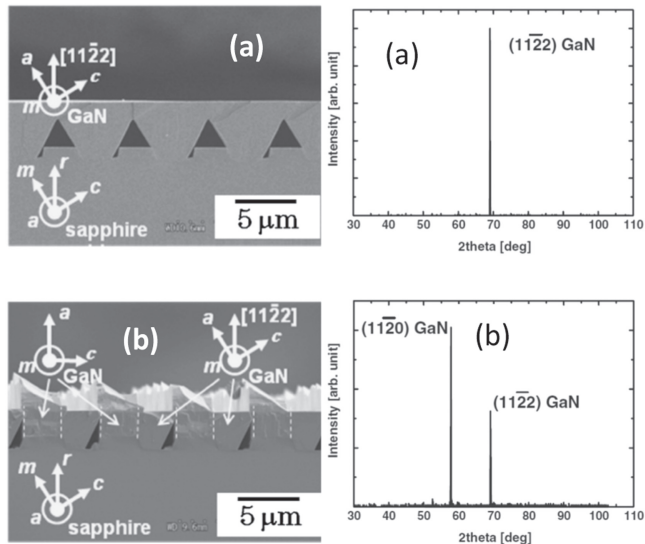


**Figure 15.** Cross-sectional SEM images and x-ray data for semi-polar (11-22) GaN grown on the patterned *r*-plane sapphire grown at (a) 1000 °C and (b) 900 °C [50]. Copyright 2009 The Japan Society of Applied Physics.

makes the LT nucleation layer deposited on the other planes mass-transport to the *c*-plane-like sapphire sidewalls. As a result, the growth of *c*-plane GaN on the *c*-plane-like sapphire sidewall, i.e., (11-22) oriented GaN, is enhanced. It is well-known that the *c*-plane GaN grown on *c*-plane-like sapphire is thermodynamically more stable than that of *a*-plane GaN grown on *r*-plane sapphire surface. Therefore, a high growth temperature is expected to not only effectively enhance the growth of the *c*-plane GaN on *c*-plane-like sapphire, but also to suppress the growth of *a*-plane GaN on the *r*-plane sapphire surface. Figure 15 confirms this conclusion by demonstrating that the growth at 1000 °C leads to the formation of a smooth surface and singular semi-polar (11-22) GaN, while both the *a*-plane GaN and *c*-plane GaN are formed when the growth is performed at 900 °C, leading to a rough surface.

It is worth highlighting that a fairly large angle exists, approximately 12.4°, between the inclined *c*-plane-like sidewalls and the *c*-plane of the *r*-plane sapphire substrate. As a result, major defects may be generated and thus further optimisation in fabricating such grooved patterns is necessary. Due to the intrinsic chemical inertness of sapphire, it would not be easy to control the inclination angle of the formed *c*-plane-like sidewalls by a standard dry-etching technique.

The growth of semi-polar (11-22) GaN was first demonstrated by Chen *et al* [46] who reported the fabrication of such grooved patterns on *r*-plane sapphire using a chemical wet-etching process. A SiO<sub>2</sub> mask, with 6 μm window regions and 1 μm mask regions, orientated along the [11-20] direction was deposited on *r*-plane sapphire using a standard photolithography technique. A H<sub>3</sub>PO<sub>4</sub>-based solution was then used to selectively etch the patterned sapphire substrates at 300 °C for 5 min. Finally a buffered oxide etch solution (NH<sub>4</sub>F:HF = 6:1) was employed in order to remove the SiO<sub>2</sub> mask for subsequent epitaxial growth. Figure 16 shows the

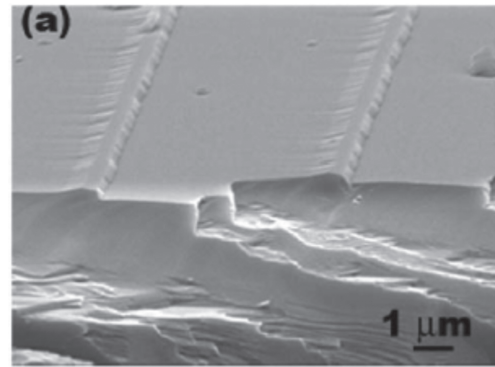


**Figure 16.** SEM image of the patterned *r*-plane sapphire fabricated using anisotropic wet-etching. This figure is reproduced from [46], with the permission of AIP Publishing.

patterned *r*-plane sapphire, demonstrating that the etched planes consist of (0001) and (1-101) facets on each side of the striped mesa. Although GaN is grown on both etched facets and the bottom (1-102) facet, leading to the formation of GaN with multiple planes, the part of the grown GaN on the inclined (0001) sapphire has been confirmed to be (11-22) GaN.

Tendille *et al* [52] have further improved the fabrication of patterned *r*-plane sapphire and have also optimised the selective growth process. They employed a similar wet-etching technique for the fabrication of the patterned *r*-plane sapphire, namely, fabrication of SiO<sub>2</sub> stripes consisting of 3 μm SiO<sub>2</sub> mask regions and 7 μm window regions, orientated along the [11-20] direction of the *m*-plane sapphire using standard photolithography. An anisotropic chemical wet-etching is then used to etch the sapphire into the grooved patterns by a mixture of H<sub>3</sub>PO<sub>4</sub> and H<sub>2</sub>SO<sub>4</sub> with a ratio of 1:3 at 270 °C for 30 min, leading to the formation of two inclined facets on each side of the SiO<sub>2</sub> stripes, the *c*-plane and (1-101) facets. Due to the long duration of wet-etching at the high temperature, each SiO<sub>2</sub> stripe has overhanging parts which need to be carefully removed before further growth. The remained SiO<sub>2</sub> masks are expected to completely block the growth of (11-20) GaN on the *r*-sapphire surface. As with the growth performed by Okada *et al*, a three-step growth procedure is used in order to form a smooth surface, namely, an initial growth for the selective growth on the inclined *c*-plane sapphire, followed by lateral growth for extending *c*-plane GaN to overlie the defect region (formed during the first step) and the final planarization/coalescence step, as shown in figure 17. In this case, a thick layer of about 10 μm is required and impressive results have been obtained; a significant improvement in crystal quality is achieved and confirmed by detailed XRD rocking curve measurements as displayed in figure 18. The FWHMs of the XRD rocking curve along the [11-2-3] direction and the [1100] direction are down to 326 and 249 arcseconds, respectively.

Such an anisotropic wet-etching process needs to be performed at a high temperature for a long time, potentially leading to a great challenge in fabrication of patterned *r*-plane

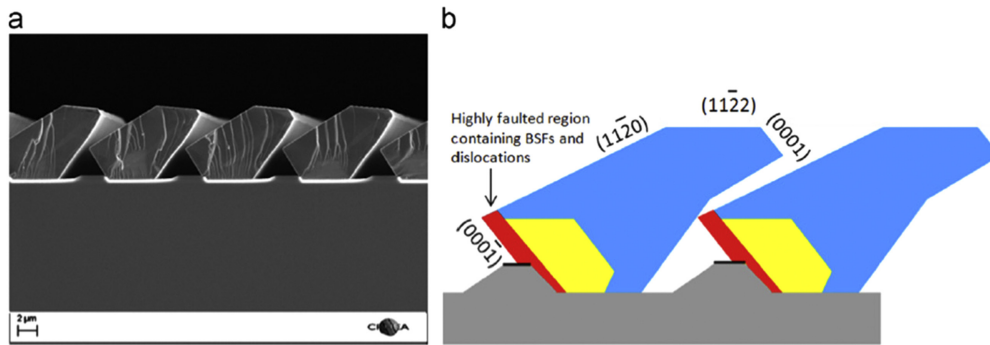


**Figure 17.** Cross-sectional SEM image of the (11-22) GaN grown on patterned *r*-plane sapphire; and schematic of the growth process. Reproduced with permission from Elsevier [52].

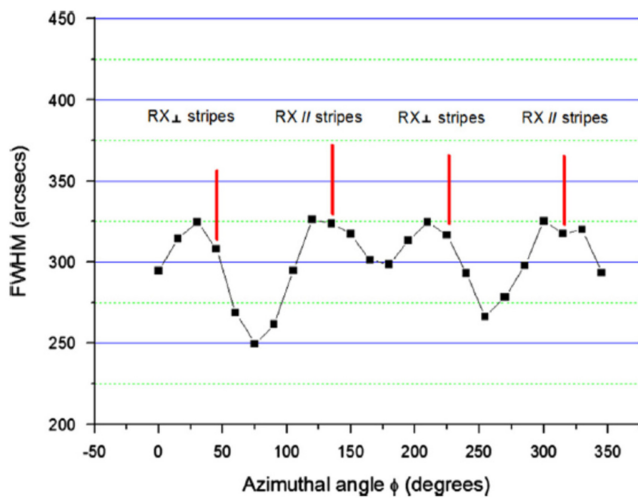


**Figure 18.** FWHM of the XRD rocking curves of the (11-22) semi-polar GaN grown on patterned *r*-plane sapphire as a function of azimuth angle. Reproduced with permission from Elsevier [52].

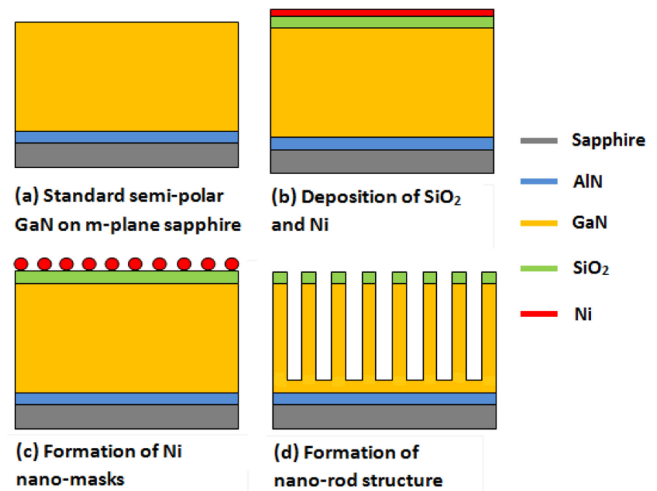


**Figure 19.** Schematic of the fabrication procedure using self-organised nickel nano masks. This figure is reproduced from [82], with the permission of AIP Publishing.

sapphire, in particular, a large size sapphire with a diameter over 2 inches.

### 3.3. Overgrowth on nano-rod array templates

The technique based on a self-organised nickel nano-mask approach has been widely employed for the fabrication of III-nitride nano-structured optoelectronics. It can also be used for GaN overgrowth. Its major advantage is due to the cost-effective fabrication of nano-rod templates and quick coalescence as a result of small gaps between nano-rods.

The Sheffield team has employed this technique originally for the fabrication of III-nitride based nano-rod array LEDs [75–80] and also applied this technique in overgrowth of non- and semi-polar GaN on sapphire [81–84]. As shown in figure 19, a SiO<sub>2</sub> thin film is initially deposited on a standard (11-22) semi-polar GaN layer directly grown on *m*-plane sapphire, followed by the thermal deposition of a thin nickel film. Subsequently the sample is annealed under flowing N<sub>2</sub> at 850 °C for 1 min. Under such conditions, the thin nickel layer evolves into self-organised nickel islands which can be tuned from 100 nm up to 1 μm in diameter on the SiO<sub>2</sub> surface. The self-organised nickel islands then serve

as a mask to etch the underlying oxide into SiO<sub>2</sub> nano-rods on the GaN surface by RIE. The SiO<sub>2</sub> nano-rods are used as a second mask and the GaN layer is dry-etched to form GaN nano-rods using an ICP technique. As an example, figure 20(a) shows a SEM image of (11-22) GaN nano-rods. A key point is to keep the SiO<sub>2</sub> masks on the top of the GaN nano-rods for subsequent overgrowth as these inhibit the adhesion of GaN onto the tops of the nano-columns.

Subsequent overgrowth initiates from the sidewalls of the nano-rod structure. The GaN growing from the sidewalls extends laterally until two adjacent growing faces meet each other. The *in situ* monitoring system shows that the GaN layer can quickly coalesce after growing just 1 μm of material. After coalescing, the GaN faces extend upwards and over the tops of the SiO<sub>2</sub> and eventually forms an atomically flat layer. A smooth surface can be achieved when the layer thickness is approximately 4 μm, demonstrating a very effective and efficient overgrowth approach compared with the conventional ELOG approaches which essentially need 10–20 μm to achieve good surface coalescence. Figure 20(b) illustrates the cross-sectional SEM images of the overgrown GaN. The SiO<sub>2</sub> and the voids both between the nano-columns and above the SiO<sub>2</sub> capped nano-rods are clearly visible. Moreover, it can be

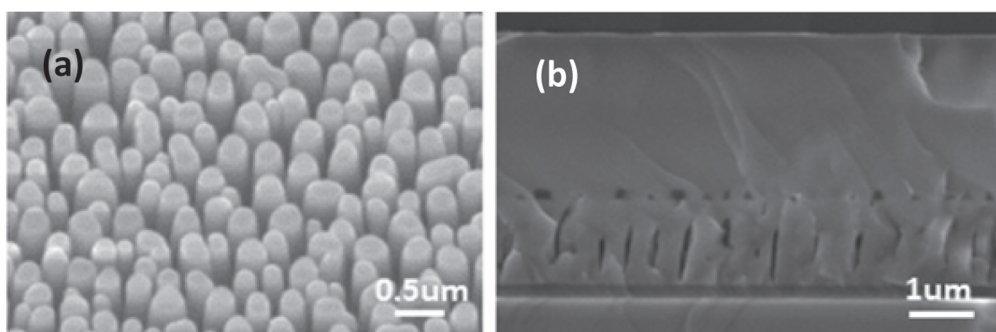


**Figure 20.** (a) SEM image of semi-polar GaN nano-rods (left); (b) cross-sectional SEM image of the semi-polar overgrown GaN (right). This figure is reproduced from [82], with the permission of AIP Publishing.

observed that the  $\text{SiO}_2$  are just located between two neighbouring voids, indicating that these voids are initially the gaps between nano-rods. Theoretically, all the dislocations and stacking faults can be effectively blocked by using this overgrowth method as both  $\text{SiO}_2$  and the voids prevent the dislocations from penetrating to the overlying GaN film. This approach is to be differentiated from other methods also using a self-organized Ni nano-mask for non-polar GaN overgrowth in which  $\text{SiO}_2$  is removed prior to growth [105].

However, unlike GaN grown along a non-polar direction, the direction of the semi-polar GaN dislocations and BSF are inclined to the GaN surface by  $58.4^\circ$ . Consequently, there are still chances for these extended defects to penetrate the top GaN layer.

XRD measurements are employed to characterize the crystal quality of the overgrown semi-polar GaN in both symmetrical and asymmetrical directions, which is compared with the semi-polar template before fabricating into the nano-rod structure. The FWHM along the on-axis (11-22) as a function of the azimuth angle ranging from  $0^\circ$  to  $180^\circ$  is shown in figure 21. The azimuth angle is defined as  $0^\circ$  if the projection of the x-ray beam onto the sample surface is parallel to the (10-10) direction, and  $90^\circ$  is defined when the incident beam is parallel to the (11-23) direction. The FWHM is reduced from 1345 to 715 arcseconds at  $0^\circ$  and 625 to 460 arcseconds at  $90^\circ$ . XRD measurements are also implemented along the (0001) off-axis for both samples. The FWHM of the semi-polar GaN template and our overgrown semi-polar GaN are 2405 and 1180 arcseconds, respectively. All of the XRD results indicate a significant reduction in the extended defects of the semi-polar overgrown GaN.

Although the approach is very cost-effective, it is very difficult to extend it in the fabrication of wafers with a diameter of  $>2$  inches as a result of the high temperature annealing process used for the formation of the self-organised nickel nano-masks. Another drawback is due to the challenge in accurately controlling either the diameter of nano-masks or patterning modes.

### 3.4. Overgrowth on regularly arrayed micro-rod templates

As mentioned above, the self-organised nickel nanomask approach has a few drawbacks which need to be resolved. Furthermore, due to the random formation mechanism of the

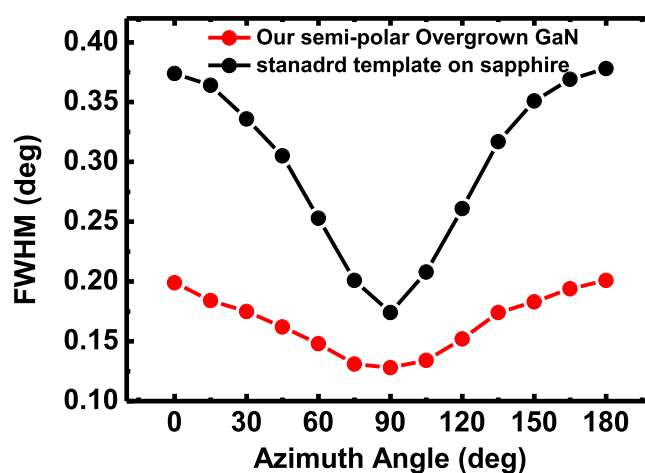


**Figure 21.** FWHMs of XRD rocking curves of the semi-polar overgrown GaN and semi-polar GaN template as a function of the azimuth angle. This figure is reproduced from [82], with the permission of AIP Publishing.

metal nano-islands, this approach hardly has extra scope for further improving the crystal quality of overgrown semi-polar GaN. In order to further improve the quality of overgrown (11-22) GaN templates and to enable the technique to extend beyond 2 inch diameter substrates, the Sheffield team developed another approach using a regular, specific array of micro-rods as opposed to the above randomly distributed nano-rods [64, 85, 86]. A standard photolithography technique which is industry-matched can be used for the mask-patterning process. As a result of utilising photolithography techniques for the mask-patterning process, the diameter of the micro-rods, the spacing between the micro-rods and the orientation of the patterning can all be precisely controlled. A  $\text{SiO}_2$  layer is initially deposited, followed by a standard photolithography patterning process and dry etching processes. Regularly arrayed  $\text{SiO}_2$  micro-rods can be achieved. Once again the  $\text{SiO}_2$  micro-rods serve as a second mask and are used to etch the GaN underneath in order to form regularly arrayed GaN micro-rod arrays with the  $\text{SiO}_2$  remaining on the top. A diameter of up to  $10 \mu\text{m}$  and spacing of the micro-rods can be accurately controlled. The overgrowth initiates from the exposed sidewalls of the micro-rods as shown in figure 22(b), and the lateral growth is dominated by the

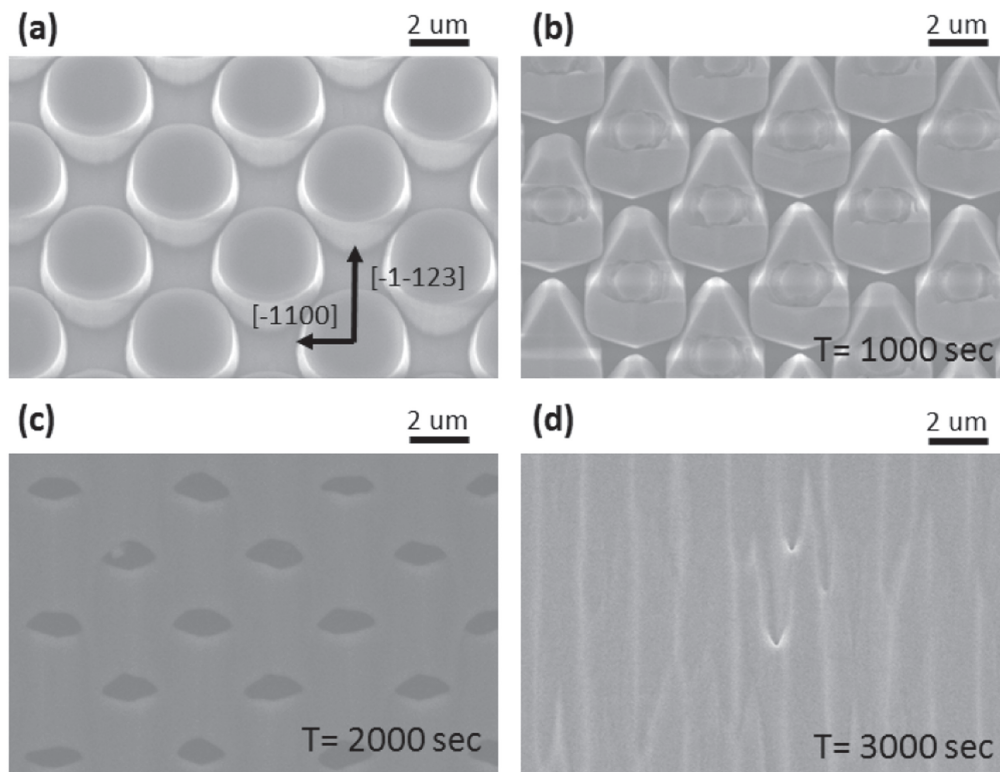


**Figure 22.** (a) Top-view SEM image of the fabricated micro-rod template; (b)–(d) evolution of the surface morphology of the overgrown layer with a growth time of 1000 s, 2000 s and 3000 s, respectively. This figure is reproduced from [86], with the permission of AIP Publishing.

growth along the  $c$ -direction and the  $[11\bar{2}0]$  or  $a$ -direction. Comparing the lengths of the two growing wings, the  $c$ -direction growth is faster than the  $a$ -direction growth. Moreover, the growth along the  $[-1100]$  or  $m$ -direction is negligible. After the coalescence of the  $c$ -direction growth and the  $a$ -direction growth facets, the GaN growth tends to move upward. When the thickness of the overgrown layer exceeds the height of the micro-rods, the growth begins to extend to cover the  $\text{SiO}_2$  masks. Although the  $m$ -direction growth is slower than growth along other directions, the specially designed pattern of the micro-rods as shown in figure 22(a) compensates the anisotropic growth rate, also facilitating another second coalescence occurring over the  $\text{SiO}_2$  masks. Eventually a full coalescence is achieved. A smooth surface can be achieved with the overgrown layer after just  $5\ \mu\text{m}$  of material have been deposited, which is faster than any other conventional ELOG techniques [89].

Figure 23(a) shows a cross-sectional SEM image of the overgrown layer where two residual voids have been observed. These were created during the initial growth stage and then coalescence stage on the  $\text{SiO}_2$  masks. In the initial stage, the growth along the  $c$ -axis effectively reduces the penetration of the defects originating from growth along the  $a$ -axis, as the  $c$ -axis growth rate is much faster than that of the  $a$ -axis, blocking the  $a$ -axis growth and thus forming the voids on the bottom. The subsequent coalescence process over the  $\text{SiO}_2$  masks further blocks the penetration of defects from the micro-rods, thus further improving crystal quality. Figure 23(b) presents XRD measurements on a  $5\ \mu\text{m}$

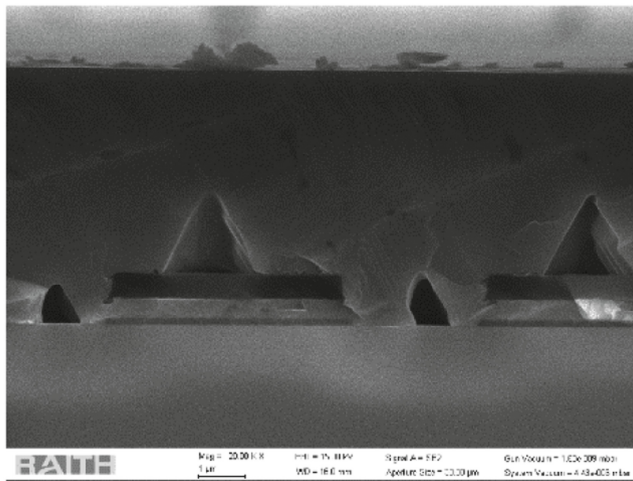
overgrown layer, showing that the FWHMs of XRD rocking curves measured along the  $[1\bar{1}00]$  (i.e., zero azimuth angle) and  $[-1\bar{1}23]$  (i.e.,  $90^\circ$  azimuth angle) directions are 360 and 250 arcseconds, respectively.

Overall, these data represent the best results on semi-polar GaN with a similar thickness grown on sapphire. This indicates that the crystal quality of such semi-polar GaN is very close to that of a standard  $c$ -plane GaN with a similar thickness grown on sapphire. Currently, the thickness of a typical GaN buffer for high brightness blue LEDs grown on  $c$ -plane sapphire is also around  $5\ \mu\text{m}$ . Therefore, it implies that such semi-polar overgrown GaN layers should be good enough for further growth of any semi-polar LED structures.

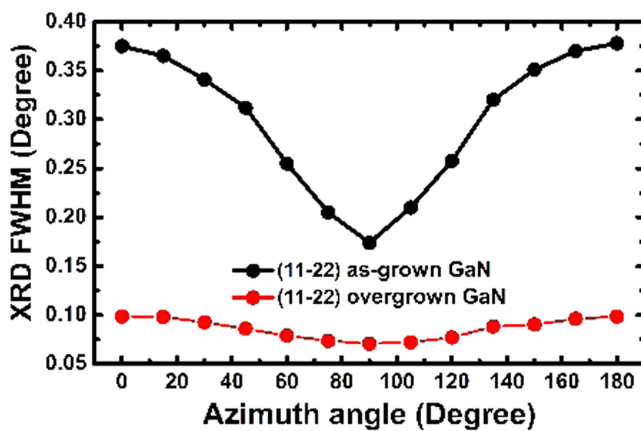
### 3.5. Growth on patterned Si

It is difficult to grow semi-polar GaN with a large inclination angle to the  $c$ -plane on a planar Si substrate due to the lack of compatible epitaxial relationship between semi-polar GaN on any orientated Si substrate. Not surprisingly, there are no reports in the literature on the growth of semi-polar (11-22) GaN on any planar Si substrates. However, given the wide availability of Si substrates and the easy patterning of Si by either dry etching or chemical wet-etching, the growth of semi-polar (11-22) GaN on patterned Si is expected to have major advantages compared with that grown on patterned  $r$ -plane sapphire.

Another challenge in the growth of GaN on Si is due to the so-called Ga melt-back etching at a high temperature; Ga



(a)



(b)

**Figure 23.** (a) Cross-sectional SEM image of the overgrown layer and (b) FWHMs of XRD rocking curves as a function of azimuth angle.

reacts with Si at high temperatures leading to a collapse during GaN growth.

Notwithstanding these technical issues, Tanikawa *et al* [55] employed anisotropic chemical etching to fabricate grooved patterning on (113) Si using a KOH solution in an attempt to grow semi-polar (11-22) GaN on Si. The fundamental mechanism is that the (111) surface of Si effectively resists the KOH etching so all other facets are etched until it reaches the (111) plane. Fortunately, the (111) surface of Si is the best for the growth of GaN; the inclination angle between the (111) and the (113) plane of the Si is 58.5 degrees, which is nearly equal to 58.4 degrees between the (11-22) and the (0001) plane of the GaN.

The fabrication of such patterned (113) Si starts with the deposition of a SiO<sub>2</sub> mask film in order to make SiO<sub>2</sub> stripe masks with optimised window regions along the [21-1] axis of (113) Si. A standard photolithography technique can be used for the patterning process. A KOH solution (25 wt%) is used to selectively etch the window regions of the (113) Si at 40 °C. Finally, as a result of the anisotropic etching nature, grooved patterning can be formed, consisting of (1-11) and

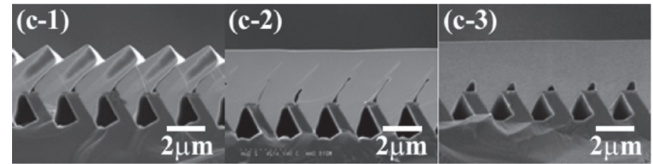


**Figure 24.** Cross-sectional SEM images of the (11-22) GaN grown on the patterned (113) Si substrates as a function of growth pressure from low to high for (c-1), (c-2), (c-3), respectively. Reproduced with permission from John Wiley & Sons [55].

(-11-1) side facets and (113) or (011) facet at the bottom. Subsequent GaN growth via MOCVD is performed on the (1-11) facets only. Figure 24 shows cross-sectional SEM images of the (11-22) GaN grown on the patterned (113) Si substrates as a function of growth pressure. In order to achieve a flat surface and avoid growth on the other facets, both the growth conditions and the patterning design need to be carefully optimised. They found that narrow window widths and deep etching depths leads to the growth of GaN only on the (1-11) side facet by eliminating the growth on the (-11-1) side facets. They concluded that a low V/III ratio and high growth pressure are important for achieving a flat surface and good crystal quality.

It is worth highlighting that a wide window would be important for further improving the crystal quality of the semi-polar GaN. Furthermore, it is essential to eliminate any Ga melt-back issue which becomes more severe with increasing growth temperature.

Very recently, the Sheffield team has developed a new approach for patterning (113) Si [87, 88] which can fundamentally resolve these issues. Figure 25 shows a SEM image of the fabricated patterned (113) Si substrate and a cross-sectional SEM image of the semi-polar (11-22) GaN grown on the patterned Si. As opposed to patterning SiO<sub>2</sub> stripe masks, the initially deposited SiO<sub>2</sub> layer is opened with quasi-square windows, obtained by a standard photolithography. The patterned SiO<sub>2</sub> serves as a second mask for subsequent anisotropic chemical wet-etching using a KOH solution, and each etched pattern manifests itself as an inverted-pyramid consisting of four (111)Si facets. Finally, extra 20 nm SiO<sub>2</sub> was selectively deposited on the substrate, covering (111), (-1-11) and (-111) facets and thus only leaving the (1-11) facets exposed. This selective deposition can be achieved by placing it at an oblique angle in an electron beam deposition chamber. By optimising the growth conditions, semi-polar (11-22) GaN with a flat surface has been obtained, which has been confirmed by detailed XRD. It is worth highlighting that the (11-22) GaN grown on such a patterned (113) Si exhibited a very low BSF density [87, 88].

#### 4. Micro-structural and electrical properties of overgrown semi-polar GaN

Regularly arrayed micro-rod templates for the overgrowth of semi-polar (11-22) GaN are designed by specifically taking the anisotropic lateral growth rates into account, as discussed

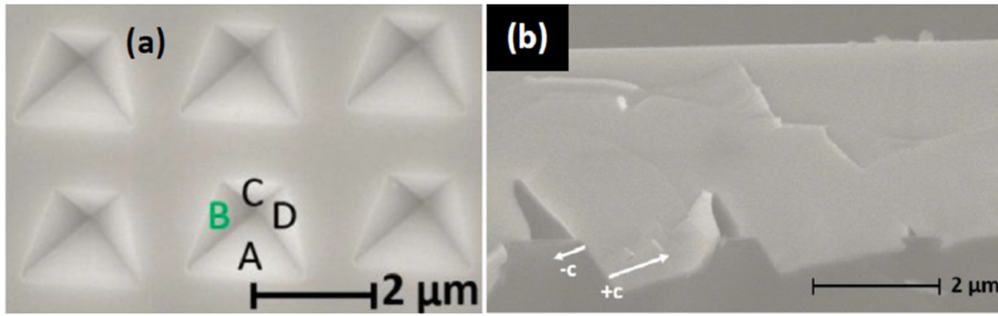


**Figure 25.** (a) Plan-view SEM image of the fabricated patterned in the (113) Si substrate; and (b) cross-sectional SEM image of the semi-polar (11-22) GaN grown on the patterned Si. Reproduced with permission from John Wiley & Sons [88].

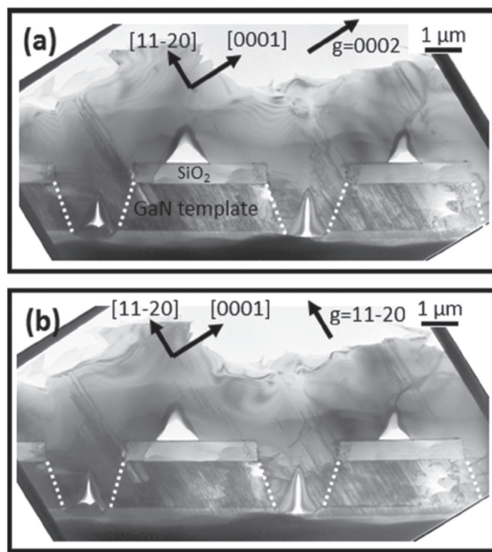


**Figure 26.** Bright field cross-sectional TEM images of overgrown GaN layers taken along the [1-100] zone-axis under a diffraction vector of (a)  $g = 0002$  and (b)  $g = 11-20$ . This figure is reproduced from [86], with the permission of AIP Publishing.

in section 3.4. Such a regularly arrayed micro-rod pattern leaves plenty of scope for further optimisation. The overgrowth of semi-polar (11-22) GaN on the regularly arrayed micro-rods is a little more complicated than those grown on patterned substrates, fabricated typically using  $\text{SiO}_2$  stripes on either  $m$ -plane sapphire or (113) Si. Consequently, gaining an understanding of the various mechanisms involved will provide valuable insight for a wide variety of different overgrowth approaches. It would be useful as a representative example for understanding the mechanisms of defect reduction in overgrown semi-polar (11-22) GaN on foreign substrates, in particular, sapphire. In this section, a study based on TEM measurements will be discussed and a model will be described.

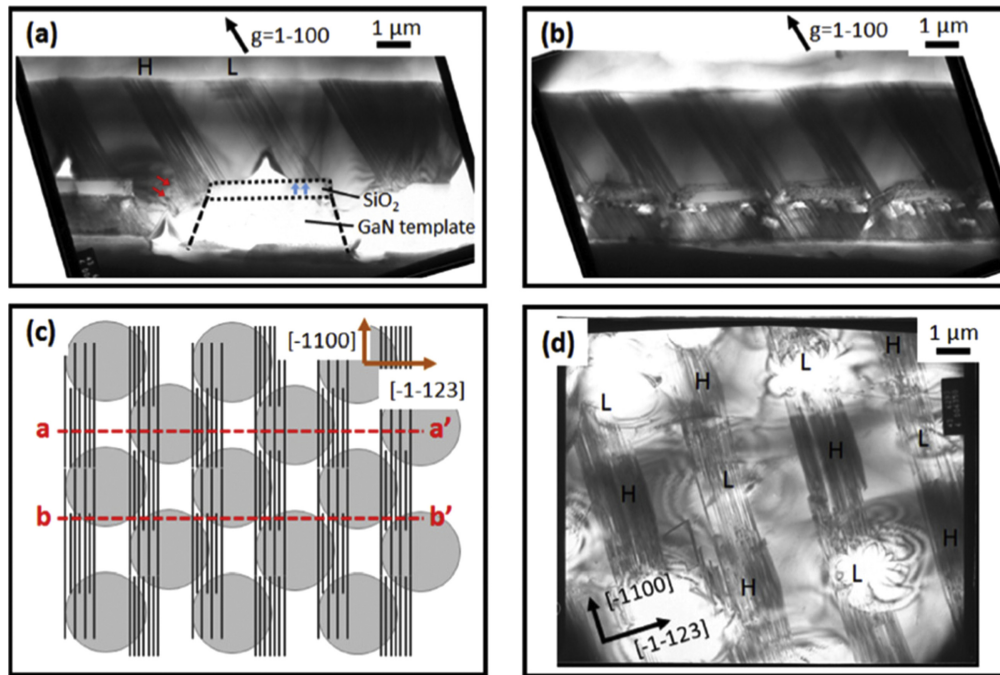
#### 4.1. Study on dislocation reduction

Figure 26(a) shows a typical bright-field cross-sectional TEM image of (11-22) semi-polar GaN overgrown on the regularly arrayed micro-rods. This TEM image was taken along [1-100] zone-axis with  $g = 0002$ , indicating  $c$ -type threading

dislocations (TDs),  $a + c$  TDs and Shockley partial dislocations. Figure 26(b) shows a typical bright-field cross-sectional TEM image taken along [1-100] zone-axis but with  $g = 11-20$ , demonstrating  $a$ -type TDs,  $a + c$  TDs and Frank partial dislocations. Both figures 26(a) and (b) show all kinds of dislocations, demonstrating that the dislocations, with an inclination angle of  $58.4^\circ$  to the surface from the GaN micro-rods under the  $\text{SiO}_2$  masks have been greatly reduced as a result of overgrowth on the micro-rod arrays. Based on an invisibility criterion [89, 90, 91, 92], dislocations are out of contrast when the product of a diffraction vector  $g$  and a dislocation displacement vector  $R$  equals zero, namely,  $g \cdot R = 0$ ; and stacking faults are invisible when the product is an integer, including zero.

The triangular-shaped voids observed in the trenches between the micro-rods are formed as a result of the first coalescence of the  $c$ -direction growth facets and the  $a$ -direction growth facets from two neighbouring micro-rods.

The voids extend from the sapphire substrate, confirming that the growth initiates from the exposed sidewalls rather than the bottom of the trenches between the micro-rods. It is important because the GaN growth from the bottom needs to be suppressed in order to prevent the defects penetrating the overlying structures. Common with the other overgrowth techniques, the GaN grown laterally along the  $c$ -direction exhibits all but free of dislocations whereas the GaN grown along the  $a$ -direction contains a number of defects. Due to the fact that the  $c$ -direction growth rate is faster than the  $a$ -direction growth rate, the  $a$ -direction growth is eventually stopped by the  $c$ -direction growth, terminating the propagation of defects from the  $a$ -direction growth. Therefore, the growth conditions favouring the  $c$ -facet growth are preferred on the early overgrowth stage, leading to an efficient reduction in dislocations and extended defects. As a result, the majority of dislocations in the GaN micro-rods are effectively prevented from penetrating by both the  $\text{SiO}_2$  masks and the  $c$ -direction growth. Only a small part of the dislocations along the  $a$ -direction propagate to the surface. Another kind of void is observed over the  $\text{SiO}_2$  mask on the top of each micro-rod as a consequence of the second coalescence along the [-12-10] and [2-1-10] directions. It is worth noting that a very small number of extra dislocations are generated due to the second coalescence. The plan-view TEM image indicates that the overall dislocation density in our overgrown (11-22) semi-



**Figure 27.** (a) and (b) Bright-field cross-sectional TEM images of the specimens prepared by cleaving differently, taken along the  $[11\bar{2}0]$  zone-axis with diffraction vector  $g = 1\bar{1}00$ ; (c) schematic of the BSF distribution on the sample surface and our micro-rod patterning. The dashed lines labelled as a-a' and b-b' depict the different cleavage directions for preparing the specimens used for TEM observation as shown (a) and (b), respectively; (d) plan-view TEM image of our  $(11\bar{2}2)$  overgrown GaN with a diffraction vector  $g = 1\bar{1}00$ . This figure is reproduced from [86], with the permission of AIP Publishing.

polar GaN is between  $1\text{--}4 \times 10^8 \text{ cm}^{-2}$ , demonstrating a significant reduction in dislocation density from the order of  $10^{10} \text{ cm}^{-2}$  in the as-grown GaN.

#### 4.2. Study on basal stacking fault reduction

BSFs as extended defects can be observed along either the  $[\bar{1}2\bar{1}0]$  or the  $[2\bar{1}\bar{1}0]$  zone-axis by tilting  $30^\circ$  from the  $[1\bar{1}00]$  zone-axis [93]. Figure 27(a) shows a typical bright-field cross-sectional TEM image taken along the  $[2\bar{1}\bar{1}0]$  direction with  $g = 1\bar{1}00$ , where BSFs appear as straight dark lines with an inclination angle of  $58.4^\circ$  to the surface. For figure 27(a), the specimen was prepared by cutting the sample along the line labelled as a-a' in figure 27(c). Figure 27(b) shows a TEM image of the specimen prepared by cutting the sample along the line labelled as b-b' in figure 27(c). The difference between the two samples is that along the a-a' line contains voids whereas along the b-b' lines does not. Apart from these physical differences, the images were recorded under identical conditions.

Since the BSFs exist in basal planes, they are impeded by the  $c$ -direction growth. As denoted by the red arrows in figure 27(a), part of the BSFs along the  $a$ -direction are blocked by the adjacent  $c$ -direction growth, leading to defect-free regions which are terminated very likely in the form of PDs and prismatic stacking faults (PSFs), while the rest of the BSFs along the  $a$ -direction are found to survive from the first coalescence process and propagate to the surface. This forms the BSF-free and BSF-containing regions distributed in a periodic form along the  $[\bar{1}1\bar{2}3]$  direction.

Figure 27(d) is a plan-view TEM image, clearly demonstrating that BSF clusters with orientation along the  $m$ -direction, i.e.  $[\bar{1}100]$ , are separated by defect-free regions along the  $[\bar{1}123]$  direction. The width of the defect-free areas is around  $1.5 \mu\text{m}$ , which is consistent with the cross-sectional TEM images as shown in figure 26(a). In addition, the distribution of these BSF clusters shows a repeat of the high BSF density areas, labelled 'H' and low BSF density areas, labelled 'L'. It means the BSFs can expand within the basal plane, propagating with a component parallel to the  $m$ -direction during the overgrowth above the  $\text{SiO}_2$  masks. During the second coalescence process, some BSFs are terminated by a formation of either PDs or PSFs, leading to a further reduction in BSF density. Consequently, this forms one area with a low BSF density, i.e., region L and another area with a high BSF density i.e. region H, appearing in a periodic form along the  $m$ -direction.

A model has been built to understand the influence of the micro-patterning on defect reduction. Figure 28(a) schematically illustrates a cross-sectional diagram of micro-rods along the  $m$ -direction. Figure 28(b) shows a simulation result, describing the relationship between the percentage of dislocation penetration from the micro-rods to the micro-rod diameter and spacing between micro-rods. The height of the micro-rods is set at  $0.4 \mu\text{m}$  and  $1.4 \mu\text{m}$  as two examples. In figure 27(b), the blue area represents a low percentage of dislocations remaining while the red area represents a high percentage. There are two low-percentage areas; one is the upper-left corner with a very small micro-rod diameter of below  $0.5 \mu\text{m}$ , and the other one is in the lower-right part with

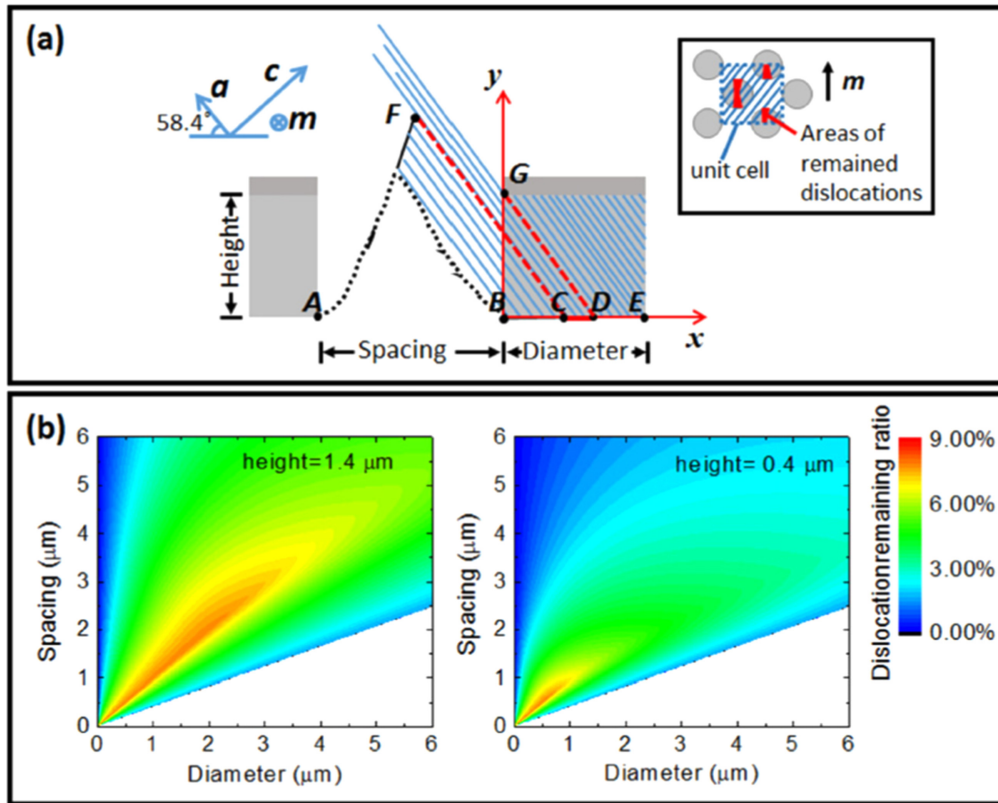


**Figure 28.** (a) Schematic diagram of our dislocation reduction model for (11-22) semi-polar overgrown GaN on micro-rod arrays along the [1-100] direction; (b) contour plots of the dislocation remaining ratio as a function of micro-rod diameter and micro-rod spacing with a micro-rod height of 1.4 and 0.4  $\mu\text{m}$ , respectively. This figure is reproduced from [86], with the permission of AIP Publishing.

a micro-rod diameter of a few microns and micro-rod spacing from 1.5 to 2.5  $\mu\text{m}$ .

Conventional photolithography typically uses an ultraviolet lighting source with a wavelength of  $\sim 300$  nm and thus it would be difficult to fabricate rod arrays with sub-micron diameter. Consequently, it is worth paying attention to the lower-right blue area, where both micro-rod diameter and micro-rod spacing are on a few micron scale. Figure 27(b) also shows that the range for the blue area increases when the micro-rod height reduces from 1.4 to 0.4  $\mu\text{m}$ , enhancing the chance for tuning either the micro-rod diameter or micro-rod spacing for effectively blocking defect penetration.

In summary, the simulation results presented in figure 27 (b) provide valuable insights that allow for further reductions in defects and thus improvements in crystal quality, such as increasing the diameter of the micro-rods, reducing the height of micro-rods and reducing the spacing between the micro-rods. Very recently, the Sheffield team has experimentally confirmed that better crystal quality in the semi-polar GaN overgrown has been obtained on micro-rods with a height of 0.4  $\mu\text{m}$  compared to micro-rods with a height of 1.4  $\mu\text{m}$ .

#### 4.3. Electrical characteristics

So far, there are only a few reports investigating the electrical properties of semi-polar GaN [94–96], possibly due to two major reasons; firstly, the crystal quality of available semi-

polar GaN is not good enough, and secondly, due to the anisotropic nature of semi-polar GaN, it would not be easy to measure its electrical properties.

The Sheffield team has performed Hall measurements via the Van der Pauw method on a series of semi-polar (11-22) GaN grown on their nano-rod array templates fabricated using the self-organized nickel nano-mask approach mentioned in section 3.3. They investigated the electrical properties of the overgrown semi-polar (11-22) GaN as a function of the diameter of nano-rods used for the fabrication of templates [94]. Generally speaking, the standard Van der Pauw approach can only be used for measuring isotropic in-plane sheet resistance, and thus isotropic carrier mobility. Therefore, it cannot be directly applied in measuring anisotropic semi-polar GaN. They employed the transmission line model (TLM) method to measure directional dependent sheet resistance and finally obtained electron mobility of semi-polar GaN in different orientations.

The free electron sheet density can still be obtained by the standard Hall measurements. The directional dependent sheet resistance was measured using the TLM method. TLM patterns along the (1-100) and (11-2-3) directions were fabricated and a Ti/Al/Ti/Au alloy was used to achieve a good ohmic contact. By measuring the resistance between each contact, the directional dependent sheet resistance can be obtained. The directional dependent electron mobility can be

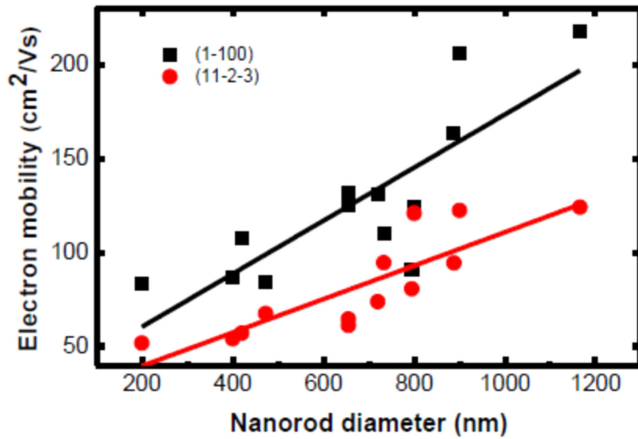


**Figure 29.** Electron mobility as a function of the nano-rod diameter in different directions. Reproduced with permission from John Wiley & Sons [94].

deduced from the equation;

$$\mu_{\text{directional}} = \frac{1}{qn_s R_{s\text{-directional}}}$$

where  $\mu_{\text{directional}}$  is directional dependent electron mobility;  $q$  is electron charge,  $n_s$  is sheet resistance and  $R_{s\text{-directional}}$  is the directional sheet resistance.

Figure 29 shows the directional dependent electron mobility of the overgrowth semi-polar (11-22) GaN, typically along both the (1-100) and the (11-2-3) directions as a function of the nano-rod diameter used for the fabrication of the templates, performed at room temperature, showing that with increasing nano-rod diameter the electron mobility can be enhanced from  $83 \text{ cm}^{-1} \text{ Vs}^{-1}$  to  $228 \text{ cm}^{-1} \text{ Vs}^{-1}$  along the (1-100) direction and  $51$  to  $124 \text{ cm}^{-1} \text{ Vs}^{-1}$  along the (11-2-3) direction, respectively. An electron mobility as high as  $228 \text{ cm}^{-1} \text{ Vs}^{-1}$  with an electron concentration of  $3.42 \times 10^{17} \text{ cm}^{-3}$  may be the best report for semi-polar GaN grown on sapphire so far [95, 96].

## 5. Optical properties of InGaN MQWs grown on overgrown semi-polar GaN

Current investigations of the optical properties of InGaN-based quantum well structures grown on semi-polar (11-22) GaN are mainly based on studies aimed at (i) reducing the QCSE, (ii) indium incorporation efficiency, (iii) shorter carrier recombination lifetime, (iv) enhanced indium localized effect, etc. Section 3.2 has presented some optical properties of semi-polar InGaN MQWs on both (20-21) and (11-22) GaN. This section focuses on a comparison study of the optical properties of (11-22) semi-polar and *c-plane* InGaN-based quantum well structures with a wide range of indium composition from the blue to green/yellow spectral region, in particular, on the Stokes-shift (the difference between emission energy and the absorption energy in semiconductor materials). The mechanism of the large Stokes-shift of *c-plane* InGaN quantum well structures has been debated for a long

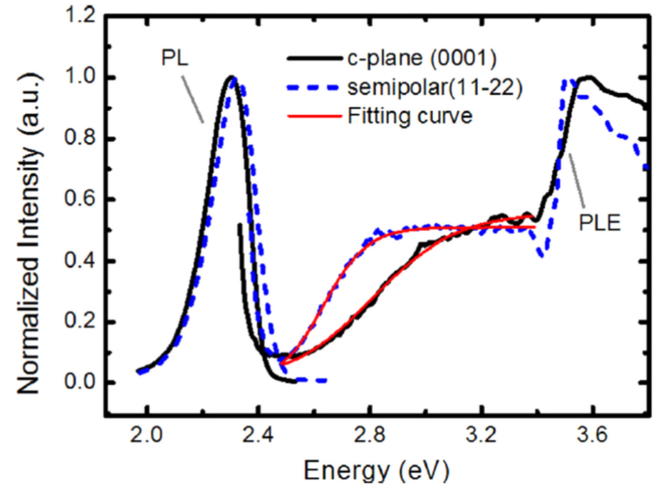


**Figure 30.** Low temperature (12 K) PL/PLE spectra of one polar (solid line) and one semi-polar (11-22) (dashed line) InGaN MQW samples with emission energy of 2.304 eV (538 nm) and 2.32 eV (534 nm), respectively. This figure is reproduced from [64], with the permission of AIP Publishing.

time. Generally speaking, a large Stokes-shift is directly related to QCSE or exciton localization effects as a result of indium fluctuation, etc. A study of the difference in the Stokes-shift of InGaN-based quantum wells grown on (11-22) semi-polar and *c-plane* GaN will contribute to an understanding of the overall optical properties of (11-22) semi-polar InGaN quantum well structures.

Basically, the Stokes-shift can be measured by photoluminescence excitation (PLE) measurements. The Sheffield team has performed a systematic study using PLE and TRPL measurements on a series of InGaN-based MQWs with a wide spectral range grown on the overgrown semi-polar GaN to investigate their optical properties [64]. The InGaN quantum well samples used were grown on micro-rod arrayed templates described in section 3.4, and their emission peak wavelengths range from 497 nm to 591 nm, covering the whole green and yellow spectral ranges. For comparison, a number of standard *c-plane* InGaN/GaN MQWs samples have also been used. Figure 30 presents PL and PLE spectra from a pair of *c-plane* (polar) and semi-polar (11-22) InGaN MQWs samples, both measured at 12 K. The PL measurements were carried out with an excitation wavelength of 350 nm, and the PLE measurements have been conducted using their emission peak energies. The two samples show similar peak emission energies located at 2.304 eV (538 nm) and 2.322 eV (534 nm), respectively. The FWHM of the PL spectrum from the semi-polar sample is 187 meV, which is larger than the 166 meV for the *c-plane* sample. Both of the PLE spectra show that there are two absorption edges, one associated with the GaN barriers at around 3.43 eV and the other associated with the InGaN quantum wells at the low energy side, respectively. Comparing the InGaN-related absorption edge in the two samples, it is found that the InGaN-related absorption process in the *c-plane* sample covers a wider range of energy (from 3.2 eV to 2.5 eV) than that in the semi-polar sample (from 2.87 eV to 2.5 eV) despite

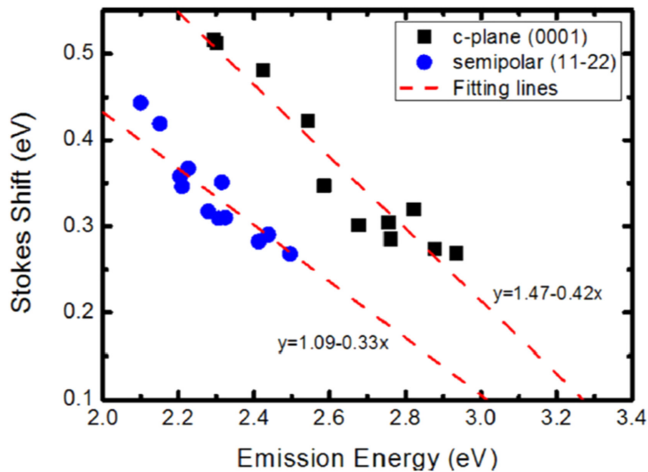


**Figure 31.** Stokes-Shift as a function of emission energy in polar (0001) and semi-polar (11-22) InGaN/GaN MQWs measured at 12 K. This figure is reproduced from [64], with the permission of AIP Publishing.

the fact that the PL spectrum of the *c-plane* sample is narrower than that of the semi-polar sample. The broadening of the quantum well absorption edge in the *c-plane* sample can be attributed to the quantum confined Franz–Keldysh (QCFK) effects [98]; due to the internal electric fields, some optical transitions that are normally forbidden have a chance to become allowed in an absorption process, broadening the quantum well absorption edge [97]. The steep absorption edge in the semi-polar sample is evidence for the reduced QCFK effects, resulting from the reduced piezoelectric fields in the quantum wells. In order to quantitatively analyze the Stokes shift, the InGaN-related absorption edges can be extracted by fitting with a sigmoidal formula [99]:

$$a = a_0 / \left[ 1 + \exp\left(\frac{E_B - E}{\Delta E}\right) \right]$$

where  $E_B$  is the effective absorption edge;  $\Delta E$  is a broadening parameter related to the Urbach tailing energy; and  $a_0$  is a constant. The fitted absorption edges are 2.813 eV and 2.634 eV for the *c-plane* and semi-polar samples, respectively. Therefore, the Stokes shift in the *c-plane* sample is 509 meV, which is larger than the 312 meV for the semi-polar sample.

Figure 31 displays the Stokes-shift values of a wide range of polar and semi-polar (11-22) MQWs samples, namely, as a function of wide emission energy. The Stokes-shift values of the *c-plane* samples linearly decrease with increasing emission energy and tend to zero at 3.50 eV (i.e. around the GaN bandgap), which is consistent with the previous work reported by other groups [106]. The semi-polar MQW samples show a lower Stokes-shift in a wide spectral range up to yellow.

Since the Stokes shift of InGaN/GaN quantum well structures can be affected by either the piezoelectric field or exciton localization effects, or both, low temperature TRPL measurements have been performed on these polar and semi-polar samples in order to further investigate the issue. The results show that the recombination lifetimes of the semi-

polar InGaN/GaN MQW samples is approximately one order of magnitude shorter than those observed for the *c-plane* samples, proving a significant decrease in QCSE.

Carrier localization is another major factor which could affect the Stokes-shift in InGaN/GaN MQWs. Wavelength-dependent TRPL measurements have been conducted at low temperature (7 K) to study the localization effects in these samples. For the *c-plane* samples, the obtained localization depths are 30 meV and 23 meV for the emission wavelengths at 538 nm and 490 nm, respectively, while the semi-polar samples exhibit localization energies of 45 meV at 534 nm and 42 meV at 497 nm, respectively. Although the Stokes shift values in the semi-polar samples are much smaller than those in the *c-plane* samples, the localization energies in the semi-polar samples are larger than those in the polar samples. This demonstrates that carrier localization effects only contribute a small part to the Stokes shift, compared with the presence of piezoelectric fields [100].

## 6. Long wavelength InGaN/GaN emitters on overgrown semi-polar GaN

To date, there have been few reports on the growth of long wavelength (green/yellow spectral region) emitters grown on (11-22) semi-polar GaN. Hikosaka *et al* reported (11-22) InGaN/GaN LEDs with an emission wavelength of 420 nm–460 nm on patterned (113) Si substrates in 2008 [54]. The patterned (113)Si substrates were fabricated using SiO<sub>2</sub> stripe masks with optimised window regions along the [21–1] axis of the (113)Si as discussed in section 3.5. Their LED structures consisted of a SQW active region with a 4 nm InGaN well sandwiched by 8 nm GaN barriers, followed by a 20 nm Mg-doped AlGaIn electron blocking layer and a 150 nm Mg-doped GaN layer and a final 20 nm Mg-doped GaN contact layer. As expected, their (11-22) LEDs show a significant reduction in blue-shift with increasing injection current as a result of reduced piezoelectric fields, e.g. 460 nm LEDs exhibit a 5.8 nm blue shift while a *c-plane* blue LED with a similar wavelength typically displays a 15 nm shift under similar measurement conditions. In addition the (11-22) LEDs show a broad linewidth of EL emission compared with *c-plane* LEDs. Jang *et al* reported semi-polar LEDs with an emission wavelength at 490–500 nm grown on patterned *m-plane* sapphire in 2012 [101], demonstrating an improved performance compared with semi-polar LEDs grown on planar sapphire. Okada *et al* [53] reported 506 nm green LEDs grown on patterned *r-plane* sapphire in 2012, where the stripe patterning process has been discussed above in section 3.2. As a result of the patterned substrate and air voids generated during the coalescence process, very strongly scattered green light emission was observed on the semi-polar LEDs compared with *c-plane* green LEDs, demonstrating significantly enhanced extraction efficiency due to these features. The semi-polar LED shows a blue-shift of 8.9 nm with increasing injection current from 20 mA to 100 mA, while that of the *c-plane* LED is 17.3 nm. Once again, the semi-polar LEDs also show much wider linewidth of the EL spectrum than their *c-*

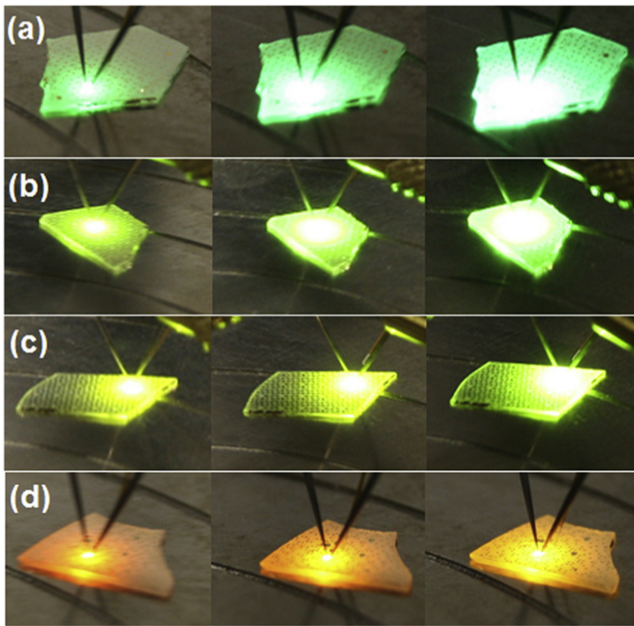


**Figure 32.** EL emission photos of (a) green, (b) yellow-green, (c) yellow, and (d) amber LEDs, taken at 5, 20, and 100 mA. This figure is reproduced from [85], with the permission of AIP Publishing.

*plane* counterparts. Interestingly, the increase in line-width of the EL spectrum of the *c-plane* LED was 5 nm with increasing injection current from 20 mA to 100 mA, while the linewidth of the (11–22) LED is only 2 nm under the same conditions.

To date, semi-polar (11–22) InGaN-based LEDs have been achieved only on free-standing (11–22) GaN substrates. (11–22) InGaN/GaN-based semi-polar laser diodes with an emission wavelength of 426 nm were reported in 2008 by the UCSB team [22]. The same group reported 445 nm semi-polar (11–22) InGaN-based laser diodes in 2012 [102], which is so far the longest wavelength laser diodes on (11–22) GaN. Optically-pumped lasing at 500 nm was achieved on semi-polar InGaN/GaN (11–22) hetero-structures on 20–25  $\mu\text{m}$  HVPE GaN templates on sapphire in 2010 [103].

Very recently, the Sheffield team has reported (11–22) semi-polar InGaN LEDs from green to amber (605 nm) on their overgrown GaN on micro-rod templates [85]. This is so far the longest wavelength LEDs reported on (11–22) semi-polar GaN, demonstrating a great advantage for using (11–22) semi-polar GaN for the growth of longer wavelength emitters and also a great potential to achieve longer wavelength laser diodes. Four InGaN SQW LED samples with different indium compositions were grown on such micro-rod templates. All the LED structures are very simple, consisting of a 4  $\mu\text{m}$  undoped GaN layer followed by a 1  $\mu\text{m}$  Si-doped n-type GaN layer, an InGaN/GaN SQW and finally a 150 nm Mg-doped p-type GaN layer. Lateral LEDs with a  $0.33 \times 0.33 \text{ mm}^2$  mesa size were fabricated by a standard photolithography technique. ITO and Ti/Al/Ti/Au alloy were used as transparent p-type contact and n-type contact, respectively. The device characterisations were performed on bare-chip devices at room temperature in a continuous wave (cw) mode.

Figure 32 shows a series of EL images for the four LEDs, each taken at 5 mA, 20 mA and 100 mA, respectively. These clearly demonstrate bright emissions in green, yellow-green, yellow and amber spectra regions, respectively. Figure 33 shows EL spectra and EL emission peak wavelengths of the four LEDs as a function of injection current demonstrating a blue shift of the wavelength with increasing injection current from 1 mA to 100 mA. For the green (11–22) LED, the shift is only 8 nm. The blue-shift slightly increases to 15 nm and 19 nm for the yellow-green and yellow LEDs respectively, which are all less than those of their *c-plane* counterparts (typically  $>30$  nm, depending on quantum well thickness). The con-focal PL measurements indicate that a very strong exciton localisation effect exists in the amber LED as a result of the very high indium content [107]. The shoulder peak of the amber LED could originate from the significantly enhanced localised states and thus part of the blue-shift at low injection current could be due to the carrier filling of low-energy localised potentials.

Figure 34(a) shows the typical current–voltage curves, displaying a standard behaviour of InGaN-based LEDs with a typical turn-on voltage of 3.0 V–3.4 V at 20 mA injection current for the green, yellow-green, and yellow LEDs, which are comparable to *c-plane* InGaN-based LEDs. For the amber LED, the voltage at 20 mA is higher, very likely related to the p-type GaN. Figure 34(b) shows normalised external quantum efficiency (*EQE*) as a function of injection current. The *EQE* at 100 mA drops down to 87%, 80%, 79%, and 69% of the maximum for the green, yellow-green, yellow, and amber LEDs, respectively. As a reference, the *EQE* of a *c-plane* green LED fabricated based on commercial LED wafers starts to decrease from a very low current (3 mA) and then drops down to 49% of the maximum at 100 mA. It suggests that the efficiency-droop issue could be potentially reduced through growth and fabrication of (11–22) semi-polar LEDs.

The *I–V* characteristics as shown in figure 34 are encouraging, as it implies that BSFs which are supposed to affect the electrical properties do not appear to be an issue. Clearly, the LED structures have not been optimised yet so there is scope to further improve these long emission wavelength LEDs.

In spite of the above demonstration of LEDs with an emission wavelength up to amber, it is a long way to go in order to achieve InGaN-based long wavelength such as green, yellow or even red emitters with similar quantum efficiency to the current state-of-the-art for blue emitters which is above 80% [110]. On (11–22) free-standing substrates, UCSB has reported 563 nm LEDs with an external quantum efficiency of 13.4%, demonstrating an encouraging result.

## 7. Summary and outlook

Homo-epitaxial growth is ideal and has been widely used in the growth of III-V semiconductors except III-nitrides and as a result the last three to four decades have seen huge successes in III-V semiconductors, especially for GaAs. The research activity on ‘lattice mismatched hetero-epitaxy’

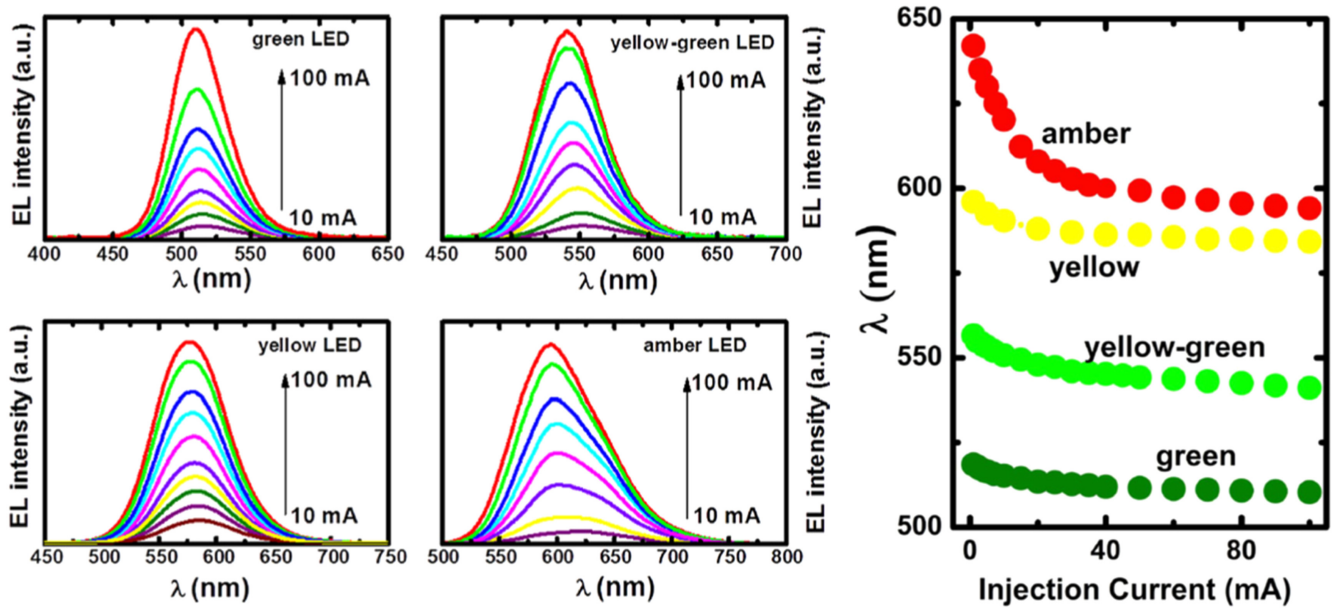


**Figure 33.** EL spectra (left) and EL emission peak wavelength (right) as a function of injection current. This figure is reproduced from [85], with the permission of AIP Publishing.

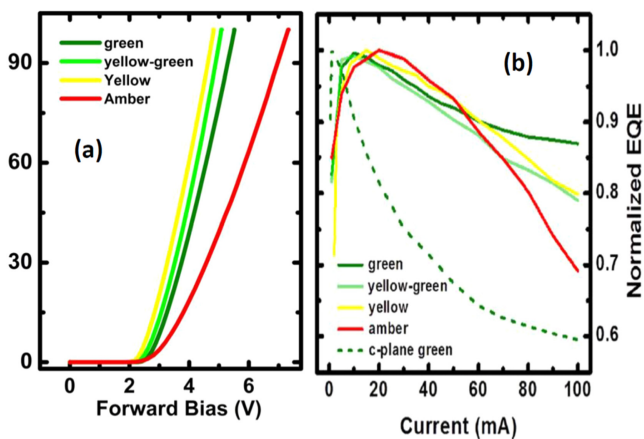


**Figure 34.** (a) Typical current–voltage ( $I$ - $V$ ) curves; (b) normalised external quantum efficiency ( $EQE$ ) as a function of injection current. This figure is reproduced from [85], with the permission of AIP Publishing.

started a long time ago, early GaP grown on Si and GaAs on Si, now III-nitrides on sapphire or Si. Clearly, the last two decades have seen a great success in lattice mismatched hetero-epitaxy, represented by GaN-on-sapphire. However, it is mainly limited to  $c$ -plane GaN on (0001) sapphire, the lowest index sapphire. Although high brightness blue LEDs have been achieved and commercialised, the crystal quality of GaN is still a great challenge for some optoelectronics which need to work under extreme conditions, for example, laser diodes which need to operate under high injection current and photodetectors which need to operate at high bias to detect a weak signal. In both cases, the crystal quality of GaN on sapphire or Si may not be good enough. The same story occurs with semi-polar or non-polar GaN-based optoelectronics, but it is even worse, as the crystal quality of semi-polar or nonpolar GaN directly grown on sapphire is much

worse than that on  $c$ -plane GaN. Therefore, it is important to devote considerable effort to improving the crystal quality of semi-polar and non-polar GaN in a cost-effective way on a large wafer in order to meet industrial requirements.

In terms of achieving InGaN-based long wavelength emitters, the (101-1) GaN surface would be best, as it enables the highest indium incorporation among all the GaN planes. However, it suffers from some fundamental challenges in growth. The (20-21) GaN surface would be best for the growth of semi-polar laser diodes, but it exhibits the same indium incorporation properties as  $c$ -plane GaN. In light of the above, the best compromise orientation for achieving longer wavelength emitters is (11-22) GaN, provided it can be manufactured with high crystal quality and on large size wafers. Of course, towards longer wavelength laser diodes, a number of great challenges need to be overcome. It is worth highlighting that these challenges could be met through further optimising or developing new growth methods, for example, the enhanced indium composition fluctuation on (11-22) GaN might be reduced or minimised by reducing the thickness; the reduced critical thickness for the formation of misfit dislocation might be mitigated through optimising the design of hetero-structures. Optically pumped stimulated emission at 514 nm (pure green) on semi-polar (11-22) InGaN MQWs has been achieved [104], which is very encouraging and promising towards lasing with longer wavelengths on (11-22) GaN.

Currently, there is a gap between III-nitrides and other III-V semiconductors. Integrating III-nitrides and other III-V semiconductors through epitaxial growth would lead to a revolution in the field of compound semiconductors, which may result in a breakthrough in the growth and fabrication of new devices which have never appeared. Hopefully, (11-22) GaN will play an important role in bridging the gap.

## Acknowledgments

This work was supported by the UK Engineering and Physical Sciences Research Council (EPSRC) via Grant Nos. EP/M015181/1 and EP/L017024/1. The author thanks Dr Carl Griffiths who read through the manuscript.

## References

- [1] Amano H, Sawaki N, Akasaki I and Toyoda Y 1986 Metal-organic vapor phase epitaxial growth of a high quality GaN film using an AlN buffer layer *Appl. Phys. Lett.* **48** 354
- [2] Amano H, Kito M, Hiramatsu K and Akasaki I 1989 P-type conduction in Mg-doped GaN treated with low-energy electron beam irradiation *Jpn. J. Appl. Phys.* **28** L2112
- [3] Nakamura S, Mukai T and Senoh M 1994 Candela-class high-brightness InGaN/AlGaIn double-heterostructure blue-light-emitting diodes *Appl. Phys. Lett.* **64** 1687
- [4] Avramescu A, Lermer T, Müller J, Eichler C, Bruederl G, Sabathil M, Lutgen S and Strauß U 2010 True green laser diodes at 524 nm with 50 mW continuous wave output power on *c*-plane GaN *Appl. Phys. Express* **3** 061003
- [5] Nakamura S, Senoh M, Iwasa N and Nagahama S 1995 High-brightness InGaN blue, green and yellow light emitting diodes with quantum well structures *Jpn. J. Appl. Phys.* **34** L797
- [6] Mukai T, Narimatsu H and Nakamura S 1998 Amber InGaIn based light-emitting diodes operable at high ambient temperatures *Jpn. J. Appl. Phys.* **37** L479
- [7] Mukai T, Yamada M and Nakamura S 1999 Characteristics of InGaIn-based UV/blue/green/amber/red light-emitting diodes *Jpn. J. Appl. Phys.* **38** 3976
- [8] Deisseroth K 2011 Optogenetics *Nat. Methods* **8** 26
- [9] Ling S-C, Lu T-C, Chang S-P, Chen J-R, Kuo H-C and Wang S-C 2010 Low efficiency droop in blue-green *m*-plane InGaIn/GaN light emitting diodes *Appl. Phys. Lett.* **96** 231101
- [10] Kioupakis E, Rinke P, Delaney K T and Van de Walle C G 2011 Indirect Auger recombination as a cause of efficiency droop in nitride light-emitting diodes *Appl. Phys. Lett.* **98** 161107 and references therein
- [11] Komine T and Nakagawa M 2004 Fundamental analysis for visible-light communication system using LED lights *IEEE Trans. Consum. Electron.* **50** 100 (the pioneering work on VLC); and references therein
- [12] Takeuchi T, Amano H and Akasaki I 2000 Theoretical study of orientation dependence of piezoelectric effects in wurtzite strained GaInN/GaN heterostructures and quantum wells *Jpn. J. Appl. Phys.* **39** 413
- [13] McLaurin M, Mates T E and Speck J S 2005 Molecular-beam epitaxy of *p*-type *m*-plane GaN *Appl. Phys. Lett.* **86** 262104
- [14] Tsuchiya Y, Okadome Y, Honshio A, Miyake Y, Kawashima T, Iwaya M, Kamiyama S, Amano H and Akasaki I 2005 Control of *p*-type conduction in *a*-plane GaN grown on sapphire *r*-plane substrate *Jpn. J. Appl. Phys.* **44** L1516
- [15] Akiyama T, Ammi D, Nakamura K and Ito T 2009 Stability of magnesium-incorporated semipolar GaN (1011) surfaces *Jpn. J. Appl. Phys.* **48** 110202
- [16] Park S H 2002 Crystal orientation effects on electronic properties of wurtzite InGaIn/GaN quantum wells *J. Appl. Phys.* **91** 9904
- [17] Sasaki T and Zembutsu S 1987 Substrate-orientation dependence of GaN single-crystal films grown by metalorganic vapor-phase epitaxy *J. Appl. Phys.* **61** 2533
- [18] Waltereit P, Brandt O, Trampert A, Grahn H T, Menniger J, Ramsteiner M, Reiche M and Ploog K H 2000 Nitride semiconductors free of electrostatic fields for efficient white light-emitting diodes *Nature (London)* **406** 865
- [19] Ravash R, Blaesing J, Dadgar A and Krost A 2010 Semipolar single component GaN on planar high index Si(11h) substrates *Appl. Phys. Lett.* **97** 142102
- [20] Okamoto K, Kashiwagi J, Tanaka T and Kubota M 2009 Nonpolar *m*-plane InGaIn multiple quantum well laser diodes with a lasing wavelength of 499.8 nm *Appl. Phys. Lett.* **94** 071105
- [21] Enya Y *et al* 2009 531 nm green lasing of InGaIn based laser diodes on semi-polar (2021) free-standing GaN substrates *Appl. Phys. Express* **2** 082101
- [22] Asamizu H, Saito M, Fujito K, Speck J S, DenBaars S P and Nakamura S 2008 Demonstration of 426 nm InGaIn/GaN laser diodes fabricated on free-standing semipolar (1122) gallium nitride substrates *Appl. Phys. Express* **1** 091102
- [23] Yoshizumi Y *et al* 2009 Continuous-wave operation of 520 nm green InGaIn-based laser diodes on semi-polar (2021) GaN substrates *Appl. Phys. Express* **2** 092101
- [24] Adachi M *et al* 2010 Low threshold current density InGaIn based 520–530 nm green laser diodes on semi-polar (2021) free-standing GaN substrates *Appl. Phys. Express* **3** 121001
- [25] Fujito K K, Kubo S and Fujimura I 2009 Development of bulk GaN crystals and nonpolar/semipolar substrates by HVPE *MRS Bull.* **34** 313
- [26] Fujito K, Kubo S S, Nagaoka H, Mochizuki T, Namita H H and Nagao S 2009 Bulk GaN crystals grown by HVPE *J. Cryst. Growth* **311** 3011
- [27] Masui H, Nakamura S, DenBaars S P and Mishra U K 2010 Nonpolar and semipolar III-nitride light-emitting diodes: achievements and challenges *IEEE Trans. Electron Devices* **57** 88 (review paper)
- [28] Pereira S, Correia M R, Pereira E, O'Donnell K P, Alves E, Sequeira A D, Franco N, Watson I M and Deatcher C J 2002 Strain and composition distributions in wurtzite InGaIn/GaN layers extracted from x-ray reciprocal space mapping *Appl. Phys. Lett.* **80** 3913
- [29] Shimizu M, Kawaguchi Y, Hiramatsu K and Sawaki N 1997 Metalorganic vapor phase epitaxy of thick InGaIn on sapphire substrate *Jpn. J. Appl. Phys.* Part 1 **36** 3381
- [30] Sonderegger S, Feltin E, Merano M, Crottini A, Carlin J F, Sachot R, Deveaud B, Grandjean N and Ganière J D 2006 High spatial resolution picosecond cathodoluminescence of InGaIn quantum wells *Appl. Phys. Lett.* **89** 232109
- [31] Koleske D D, Lee S R, Crawford M H, Coltrin M E and Fini P T Semi-polar GaN Materials Technology for High IQE Green LEDs' *Sandia Report*, June 2013
- [32] Northrup J E 2009 GaN and InGaIn (11-22) surfaces: group-III adlayers and indium incorporation *Appl. Phys. Lett.* **95** 133107
- [33] Ranalli F, Parbrook P J, Bai J, Lee K B, Wang T and Cullis A G 2009 Non-polar AlN and GaN/AlN on *r*-plane sapphire *Phys. Stat. Sol. C* **6** S780
- [34] Wernicke T, Netzel C, Weyers M and Kneissl M 2008 Semipolar GaN grown on *m*-plane sapphire using MOVPE *Phys. Stat. Sol. C* **5** 1815
- [35] Kamiyama S, Honshio A, Kitano T, Iwaya M, Amano H, Akasaki I, Kinoshita H and Shiomi H 2005 GaN growth on (30-38) 4H-SiC substrate for reduction of internal polarization *Phys. Stat. Sol. C* **2** 2121
- [36] Baker T J, Haskell B A, Wu U F, Fini P T, Speck J S and Nakamura S 2005 Characterization of planar semipolar gallium nitride films on spinel substrates *Jpn. J. Appl. Phys.* **44** L 920
- [37] Hikosaka T, Narita T, Honda Y, Yamaguchi M and Sawaki N 2004 Optical and electrical properties of (1-101) GaN grown on a 7° off-axis (001) Si substrate *Appl. Phys. Lett.* **84** 4717

- [38] Bessolov I V N, Konenkova I E V, Kukushkin S A, Osipov A V and Rodin S N 2014 Semipolar gallium nitride on Si: technology and properties *Rev. Adv. Mater. Sci.* **38** 75
- [39] Schwaiger S, Argut I, Wunderer T, Rösch R, Lipski F, Biskupek J, Kaiser U and Scholz F 2010 Planar semipolar (10-11) GaN on (11-23) sapphire *Appl. Phys. Lett.* **96** 231905
- [40] Schulze F, Dadgar A, Bläsing J and Krost A 2004 Influence of buffer layers on metalorganic vapor phase epitaxy grown GaN on Si (001) *Appl. Phys. Lett.* **84** 4747
- [41] Sharma R, Pattison P M, Masui H, Farrell R M, Baker T J, Haskell B A, Wu F, DenBaars S P, Speck J S and Nakamura S 2005 Demonstration of a semipolar (10-1-3) InGaN/GaN green light emitting diode *Appl. Phys. Lett.* **87** 231110
- [42] Baker T J, Haskell B A, Wu U F, Speck J S and Nakamura S 2005 Characterization of planar semipolar gallium nitride films on sapphire substrates *Jpn. J. Appl. Phys.* **45** L154
- [43] Frentrup M, Ploch S, Pristovsek M and Kneissl M 2011 Crystal orientation of GaN layers on (10-10) *m-plane* sapphire *Phys. Stat. Sol. B* **248** 583
- [44] Lee H, Mitsunari T, Honda Y and Amano H 2015 Semi-polar GaN (10-13) grown on nominal Si (001) substrate with sputtered AlN buffer layer *IEICE* **115** No 63
- [45] Ravash R, Bläsing J, Hempel T, Noltemeyer M, Dadgar A, Christen J and Krost A 2009 Metal organic vapor phase epitaxy growth of single crystalline GaN on planar Si (211) substrates *Appl. Phys. Lett.* **95** 242101
- [46] Chen H-G, Ko T-S, Ling S-C, Lu T-C, Kuo H-C, Wang S-C, Wu Y-H and Chang L 2007 Dislocation reduction in GaN grown on stripe patterned *r-plane* sapphire substrates *Appl. Phys. Lett.* **91** 021914
- [47] Furuya H, Okada N and Tadatomo K 2012 Growth of (11-22) GaN on shallowly etched *r-plane* patterned sapphire substrates *Phys. Stat. Sol. C* **9** 568
- [48] Furuya H, Hashimoto Y, Yamane K, Okada N and Tadatomo K 2014 Characterization of (11-22) GaN grown using two-step growth technique on shallowly etched *r-plane* patterned sapphire substrates *J. Cryst. Growth* **391** 41
- [49] de Mierry P, Kappei L, Tendille F, Vennegues P, Leroux M and Zuniga-Perez J 2016 Green emission from semipolar InGaN quantum wells grown on low-defect (11-22) GaN templates fabricated on patterned *r-sapphire* *Phys. Stat. Sol. B* **253** 105
- [50] Okada N, Kurisu A, Murakami K and Tadatomo K 2009 Growth of semipolar (11-22) GaN layer by controlling anisotropic growth rates in *r-plane* patterned sapphire substrate *Appl. Phys. Express* **2** 091001
- [51] Song K-R, Lee J-H, Han S-H, Yi H-R and Lee S-N 2013 Study of epitaxial lateral overgrowth of semipolar (11-22) GaN by using different SiO<sub>2</sub> pattern sizes *MRS Bull.* **48** 5088
- [52] Tendille F, DeMierry P, Vennéguès P, Chenot S and Teisseire M 2014 Defect reduction method in (11-22) semipolar GaN grown patterned sapphire substrate by MOCVD: toward heteroepitaxial semipolar GaN free of basal stacking faults *J. Cryst. Growth* **404** 177
- [53] Okada N, Uchida K, Miyoshi S and Tadatomo K 2012 Green light-emitting diodes fabricated on semipolar (11-22) GaN on *r-plane* patterned sapphire substrate *Phys. Stat. Sol. A* **209** 469
- [54] Hikosaka T, Tanikawa T, Honda Y, Yamaguchi M and Sawaki N 2008 Fabrication and properties of semi-polar (1-101) and (11-22) InGaN/GaN light emitting diodes on patterned Si substrates *Phys. Stat. Sol. C* **5** 2234
- [55] Tanikawa T, Hikosaka T, Honda Y, Yamaguchi M and Sawaki N 2008 Growth of semi-polar (11-22) GaN on a (113)Si substrate by selective MOVPE *Phys. Stat. Sol. C* **5** 2966
- [56] Murase T, Tanikawa T, Honda Y, Yamaguchi M, Amano H and Sawaki N 2011 Drastic reduction of dislocation density in semipolar (11-22) GaN stripe crystal on Si substrate by dual selective metal-organic vapor phase epitaxy *Jpn. J. Appl. Phys.* **50** 01AD04
- [57] Okada N, Oshita H, Yamane K and Tadatomo K 2011 High-quality (20-21) GaN layers on patterned sapphire substrate with wide-terrace *Appl. Phys. Lett.* **99** 242103
- [58] Arauchi T, Takeuchi S, Hashimoto Y, Nakamura Y, Yamane K, Okada N, Imai Y, Kimura S, Tadatomo K and Sakai A 2015 Crystalline property analysis of semipolar (20-21) GaN on (22-43) patterned sapphire substrate by x-ray microdiffraction and transmission electron microscopy *Phys. Stat. Sol. B* **252** 1149
- [59] Khoury M, Leroux M, Nemoz M, Feillet G, Zúñiga-Pérez J and Vennéguès P 2015 Growth of semipolar (20-21) GaN layers on patterned Si (114) 1° off by metal organic vapor phase epitaxy *J. Cryst. Growth* **419** 88
- [60] Becerra D L, Zhao Y, Oh S H, Pynn C D, Fujito K, DenBaars S P and Nakamura S 2014 High-power low-droop violet semipolar (30-3-1) InGaN/GaN light-emitting diodes with thick active layer design *Appl. Phys. Lett.* **105** 171106
- [61] Wernicke T, Schade L, Netzel C, Rass J, Hoffmann V, Ploch S, Knauer A, Weyers M, Schwarz U and Kneissl M 2012 Indium incorporation and emission wavelength of polar, nonpolar and semipolar InGaN quantum wells *Semicond. Sci. Technol.* **27** 024014
- [62] Zhao Y *et al* 2012 Indium incorporation and emission properties of nonpolar and semipolar InGaN quantum wells *Appl. Phys. Lett.* **100** 201108
- [63] Funato M, Kaneta A, Kawakami Y, Enya Y, Nishizuka K, Ueno M and Nakamura T 2010 Weak carrier/exciton localization in InGaN quantum wells for green laser diodes fabricated on semi-polar (20-21) GaN substrates *Appl. Phys. Express* **3** 021002
- [64] Zhang Y, Smith R M, Hou Y, Xu B, Gong Y, Bai J and Wang T 2016 Stokes shift in semi-polar (11-22) InGaN/GaN multiple quantum wells *Appl. Phys. Lett.* **108** 031108
- [65] Ueda M, Kojima K, Funato M, Kawakami Y, Narukawa Y and Mukai T 2006 Epitaxial growth and optical properties of semipolar (112-2) GaN and In GaN/GaN quantum wells on GaN bulk substrates *Appl. Phys. Lett.* **89** 211907
- [66] I-hsiu H and Stringfellow G B 1996 Solid phase immiscibility in GaInN *Appl. Phys. Lett.* **69** 2701
- [67] Brown I H, Blood P, Smowton P M, Thomson J D, Olaiyola S M, Fox A M, Parbrook P J and Chow W W 2006 Time evolution of the screening of piezoelectric fields in InGaN quantum wells *IEEE J. Quantum Electron.* **42** 1202
- [68] Adachi M 2014 InGaN based green laser diodes on semipolar GaN substrate *Jpn. J. Appl. Phys.* **53** 100207
- [69] Romanov A E, Young E C, Wu F, Tyagi A, Gallinat C S, Nakamura S, DenBaars S P and Speck J S 2011 Basal plane misfit dislocations and stress relaxation in III-nitride semipolar heteroepitaxy *J. Appl. Phys.* **109** 103522
- [70] Young E C, Gallinat C S, Romanov A E, Tyagi A, Wu F and Speck J S 2010 Critical thickness for onset of plastic relaxation in (11-22) and (20-21) semipolar AlGaIn heterostructures *Appl. Phys. Express* **3** 111002
- [71] Ploch S, Wernicke T, Thalmair J, Lohr M, Pristovsek M, Zweck J, Weyers M and Kneissl M 2012 Topography of (2021) AlGaIn, GaN and InGaIn layers grown by metal-organic vapor phase epitaxy *J. Cryst. Growth* **356** 70
- [72] Zhao Y, Wu F, Yang T-J, Wu Y-R, Nakamura S and Speck J S 2014 Atomic-scale nanofacet structure in semipolar (20-2-1) and (20-21) InGaIn single quantum wells *Appl. Phys. Express* **7** 025503
- [73] Ni X, Özgür Ü, Baski A A, Morkoç H, Zhou L, Smith D J and Tran C A 2007 Epitaxial lateral overgrowth of (11-22)

- semipolar GaN on (1-100) *m-plane* sapphire by metalorganic chemical vapor deposition *Appl. Phys. Lett.* **90** 182109
- [74] Song K-R, Lee J-H, Han S-H, Yi H-R and Lee S-N 2013 Study of epitaxial lateral overgrowth of semipolar (11-2 2) GaN by using different SiO<sub>2</sub> pattern sizes *MRS Bull.* **48** 5088
- [75] Wang Q, Bai J, Gong Y and Wang T 2012 Investigation of the optical properties of InGaN/GaN nanorods with different indium composition *Phys. Stat. Sol. C* **9** 620
- [76] Wang Q, Bai J and Wang T 2011 Influence of strain relaxation on the optical properties of InGaN/GaN multiple quantum well nanorods *J. Phys. D: Appl. Phys.* **44** 395102
- [77] Bai J, Wang Q and Wang T 2012 Characterization of InGaN-based nanorod light emitting diodes with different indium compositions *J. Appl. Phys.* **111** 113103
- [78] Renwick P, Tang H, Bai J and Wang T 2012 Reduced longitudinal optical phonon-exciton interaction in InGaN/GaN nanorod structures *Appl. Phys. Lett.* **100** 182105
- [79] Bai J, Wang Q and Wang T 2012 Greatly enhanced performance of InGaN/GaN nanorod light emitting diodes *Phys. Stat. Sol. A* **209** 477
- [80] Smith R, Liu B, Bai J and Wang T 2013 Hybrid III-nitride/organic semiconductor nanostructure with high efficiency non-radiative energy transfer for white light emitter *Nano Lett.* **13** 3042
- [81] Gong Y, Xing K, Bai J and Wang T 2012 Greatly improved crystal quality of non-polar GaN grown on a-plane GaN nano-rod template obtained using self-organised nano-masks *Phys. Stat. Sol. C* **9** 564
- [82] Xing K, Gong Y, Bai J and Wang T 2011 InGaN/GaN quantum well structures with greatly enhanced performance on *a-plane* GaN grown using self-organised nano-masks *Appl. Phys. Lett.* **99** 181907
- [83] Xing K, Gong Y, Yu X, Bai J and Wang T 2013 Improved crystal quality of (11-22) semi-polar GaN grown on a nano-rod template *Jpn J. Appl. Phys.* **52** 08JC03
- [84] Gong Y, Xing K, Xu B, Yu X, Li Z, Bai J and Wang T 2015 High efficiency green-yellow emission from InGaN/GaN quantum well structures grown on overgrown semi-polar (11-22) GaN on regularly arrayed micro-rod templates *ECSS Trans.* **66** 151
- [85] Bai J, Xu B, Guzman F G, Xing K, Gong Y, Hou Y and Wang T 2015 (11-22) semi-polar InGaN emitters from green to amber on overgrown GaN on micro-rod templates *Appl. Phys. Lett.* **107** 261103
- [86] Zhang Y, Bai J, Hou Y, Smith R M, Yu X, Gong Y and Wang T 2016 Defect reduction in overgrown semi-polar (11-22) GaN on a regularly arrayed micro-rod array template *AIP Adv.* **6** 025201
- [87] Bai J, Yu X, Gong Y and Wang T 2015 Depression of defects in semi-polar (11-22) GaN on patterned Si (311) substrates *Semicond. Sci. Technol.* **30** 065012
- [88] Yu X, Hou Y, Shen S, Bai J, Gong Y, Zhang Y and Wang T 2016 Semi-polar (11-22) GaN grown on patterned (113) Si substrate *Phys. Stat. Sol. C* **13** 190-4
- [89] Kriouche N, Vennegues P, Nemoz M, Nataf G and de Mierry P 2010 Stacking faults blocking process in (1 1-2 2) semipolar GaN growth on sapphire using asymmetric lateral epitaxy *J. Cryst. Growth* **312** 2625
- [90] Hino T, Tomiya S, Miyajima T, Yanashima K, Hashimoto S and Ikeda M 2000 Characterization of threading dislocations in GaN epitaxial layers *Appl. Phys. Lett.* **76** 3421
- [91] Vennegues P 2012 Defect reduction methods for III-nitride heteroepitaxial films grown along nonpolar and semipolar orientations *Semicond. Sci. Technol.* **27** 024004
- [92] Wu F, Lin Y D, Chakraborty A, Ohta H, DenBaars S P, Nakamura S and Speck J S 2010 Stacking fault formation in the long wavelength InGaN/GaN multiple quantum wells grown on *m-plane* GaN *Appl. Phys. Lett.* **96** 231912
- [93] Johnston C F, Kappers M J and Humphreys C J 2009 Microstructural evolution of nonpolar (11-20) GaN grown on (1-102) sapphire using a 3D-2D method *J. Appl. Phys.* **105** 073102
- [94] Xu B, Yu X, Gong Y, Xing K, Bai J and Wang T 2015 Study of high quality (11-22) semi-polar GaN grown on nanorod templates *Phys. Stat. Sol. B* **252** 1079
- [95] Jang S, Kim H, Kim D S, Hwang S M, Kim J and Baik K H 2013 Investigation of carrier transport properties in semipolar (11-22) GaN films with low defect density *Appl. Phys. Lett.* **103** 162103
- [96] Jung C, Jang J, Hwang J, Jeong J, Kim J, Lee K and Nam O 2013 Defect reduction in (11-22) semipolar GaN with embedded InN islands on *m-plane* sapphire *J. Cryst. Growth* **370** 26
- [97] Chichibu S F *et al* 1998 Effective band gap inhomogeneity and piezoelectric field in InGaN/GaN multi-quantum well structures *Appl. Phys. Lett.* **73** 2006
- [98] Miller D A B, Chemla D S and Schmitt-Rink S 1986 Relation between electroabsorption in bulk semiconductors and in quantum wells: the quantum-confined Franz-Keldysh effect *Phys. Rev. B* **33** 6976
- [99] O'Donnell K P, Martin R W and Middleton P G 1999 Origin of luminescence from InGaN diodes *Phys. Rev. Lett.* **82** 237
- [100] Berkowicz E, Gershoni D, Bahir G, Lakin E, Shilo D, Zolotoyabko E, Abare A C, DenBaars S P and Coldren L A 2000 Measured and calculated radiative lifetime and optical absorption of In<sub>x</sub>Ga<sub>1-x</sub>N/GaN quantum structures *Phys. Rev. B* **61** 10994
- [101] Jang J, Lee K, Hwang J, Jung J, Lee S, Lee K, Kong B, Cho H and Nam O 2012 Improvement of crystal quality and optical property in (11-22) semipolar InGaN/GaN LEDs grown on patterned *m-plane* sapphire substrate *J. Cryst. Growth* **361** 166
- [102] Hsu P S *et al* 2012 444.9 nm semipolar (11-22) laser diode grown on an intentionally stress relaxed InGaN waveguiding layer *Appl. Phys. Lett.* **100** 021104
- [103] Strittmatter A *et al* 2010 Optically-pumped lasing of semi-polar InGaN/GaN(11-22) heterostructures *Phys. Stat. Sol. C* **7** 1814
- [104] Tyagi A, Lin Y-D, Cohen D A, Saito M, Fujito K, Speck J S, DenBaars S P and Nakamura S 2008 Stimulated emission at blue-green (480 nm) and green (514 nm) wavelengths from nonpolar (*m-plane*) and semipolar (11-22) InGaN multiple quantum well laser diode structures *Appl. Phys. Express* **1** 091103
- [105] Ling S C, Chao C L, Chen J R, Liu P C, Ko T S, Lu T C, Kuo H C, Wang S C, Cheng S J and Tsay J D 2010 Crystal quality improvement of *a-plane* GaN using epitaxial lateral overgrowth on nanorods *J. Cryst. Growth* **312** 1316
- [106] Martin R W, Middleton P G, O'Donnell K P and Van der Stricht W 1999 Exciton localization and the Stokes' shift in InGaN epilayers *Appl. Phys. Lett.* **74** 263
- [107] Smith R M, Xu B, Xing K, Gong Y, Yu X, Zhang Y, Bai J and Wang T to be submitted
- [108] Keller S, Fichtenbaum N A, Furukawa M, Speck J S, DenBaars S P and Mishra U K 2007 Growth and characterization of N-polar In GaN/GaN multi-quantum wells *Appl. Phys. Lett.* **90** 191908
- [109] Akyol F, Nath D N, Gür E, Park P S and Rajan S 2011 N-polar III-nitride green (540 nm) light emitting diode *Jpn J. Appl. Phys.* **50** 052101